

Monometallic and Bimetallic Titanium κ^1 -Amidinate Complexes as Olefin Polymerization Catalysts

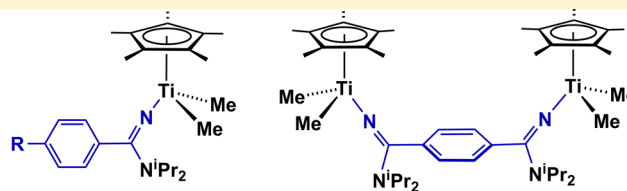
Richard A. Collins,[†] Adam F. Russell,[†] Richard T. W. Scott,^{†,‡} Raffaele Bernardo,[‡] Gerard H. J. van Doremale,[‡] Alexandra Berthoud,^{*,‡} and Philip Mountford^{*,†}

[†]Chemistry Research Laboratory, Department of Chemistry, University of Oxford, Mansfield Road, Oxford OX1 3TA, United Kingdom

[‡]Arlanxeo Netherlands B.V., Urmonderbaan 24, 6167 RD Geleen, The Netherlands

S Supporting Information

ABSTRACT: A series of cyclopentadienyl- κ^1 -amidinate titanium complexes $\text{Cp}^*\text{Ti}\{\text{NC}(\text{Ar}^R)\text{N}^i\text{Pr}_2\}\text{Me}_2$ ($\text{Ar}^R = 4\text{-C}_6\text{H}_4\text{R}$, where $\text{R} = \text{H}$ (**1-Me**), CF_3 (**5-Me**), ^tBu (**6-Me**), or NMe_2 (**7-Me**)) with different para-substituents in the amidinate ligand were synthesized and structurally characterized, along with three bimetallic analogues: $1,4\text{-C}_6\text{H}_4\{\text{C}(\text{N}^i\text{Pr}_2)\text{N}\}_2\{\text{Cp}^*\text{TiMe}_2\}_2$ (**2-Me**), $1,3\text{-C}_6\text{H}_4\{\text{C}(\text{N}^i\text{Pr}_2)\text{N}\}_2\{\text{Cp}^*\text{TiMe}_2\}_2$ (**3-Me**), and $\text{CH}_2\{1,4\text{-C}_6\text{H}_4\text{-C}(\text{N}^i\text{Pr}_2)\text{N}\}_2\{\text{Cp}^*\text{TiMe}_2\}_2$ (**4-Me**). ^{13}C NMR spectroscopy, density function theory, and the quantum theory of atoms-in-molecules were used to evaluate the donor ability of the various $\text{NC}(\text{Ar}^R)\text{N}^i\text{Pr}_2$ ligands and the influence of the Ar^R group para-substituents. Reactions of **1-Me** and certain homologues, as well as **2-Me**, with borate and borane reagents $[\text{CPh}_3][\text{BAR}^F_4]$ ($\text{Ar}^F = \text{C}_6\text{F}_5$, BAR^F_3 , in the absence or presence of Lewis bases or polar unsaturated substrates were carried out, forming adducts and migratory insertion products such as $[\text{Cp}^*\text{Ti}\{\text{NC}(\text{Ph})\text{N}^i\text{Pr}_2\}\text{Me}(\text{THF})][\text{BAR}^F_4]$, $[\text{Cp}^*\text{Ti}\{\text{NC}(\text{Ph})\text{N}^i\text{Pr}_2\}\{\text{MeC}(\text{N}^i\text{Pr})_2\}][\text{BAR}^F_4]$, and $[1,4\text{-C}_6\text{H}_4\{\text{C}(\text{N}^i\text{Pr}_2)\text{N}\}_2\{\text{Cp}^*\text{Ti}\{\text{MeC}(\text{N}^i\text{Pr})_2\}_2][\text{BAR}^F_4]_2$. Detailed olefin copolymerization studies for forming EPDM from ethylene, propylene, and certain dienes were carried out with mono- and bimetallic catalysts and borate and borane activators. Catalyst–activator effects on polymerization productivity and polymer composition relationships were mapped. Bimetallic catalysts **2** and **3** showed cooperative effects based on electronic factors, leading to enhanced propene incorporation, but unfavorable steric effects gave lower diene content. Related but less significant electronic effects on propene affinity were found for the monometallic catalysts $\text{Cp}^*\text{Ti}\{\text{NC}(\text{Ar}^R)\text{N}^i\text{Pr}_2\}\text{Me}_2$ as the Ar^R moiety para-substituents were varied.



Monometallic and cooperative bimetallic catalysts for copolymerisation

INTRODUCTION

Homogeneous olefin polymerization catalysis continues to be an area of considerable importance to both the academic and industrial communities, and a wide range of cyclopentadienyl- and noncyclopentadienyl-based transition metal systems have been described.¹ With specific regard to the Group 4 metals, the spectacular success of metallocene systems as single-site olefin polymerization catalysts² was followed by the development of a range of half-sandwich compounds, starting with the cyclopentadienyl-amido “constrained geometry catalysts” (CGCs)³ and then other systems⁴ of the type $(\eta\text{-C}_5\text{R}_5)\text{M}(\text{X})\text{R}_2$, in which the ‘X’ ligand is a heteroatom-donor moiety such as aryloxo (OAr),^{4,5} phosphinimide (NPR₃),⁶ cyclic or noncyclic guanidine (NC(NR₂)₂),⁷ ketimide (NCR₂),⁸ or κ^1 -benzamidinate (NC(Ar)NR₂).⁹ Non-cyclopentadienyl systems were also developed featuring bis(amido)-type ligands¹⁰ and their bis-(phenoxide) and related analogues,¹¹ typically incorporating additional Lewis base donors. Catalyst systems based on imido ligands with additional fac-N₃ donor ligand sets were also developed,¹² building on and exploiting the isolobal analogy between cyclopentadienide and these N-donor ligand sets.¹³

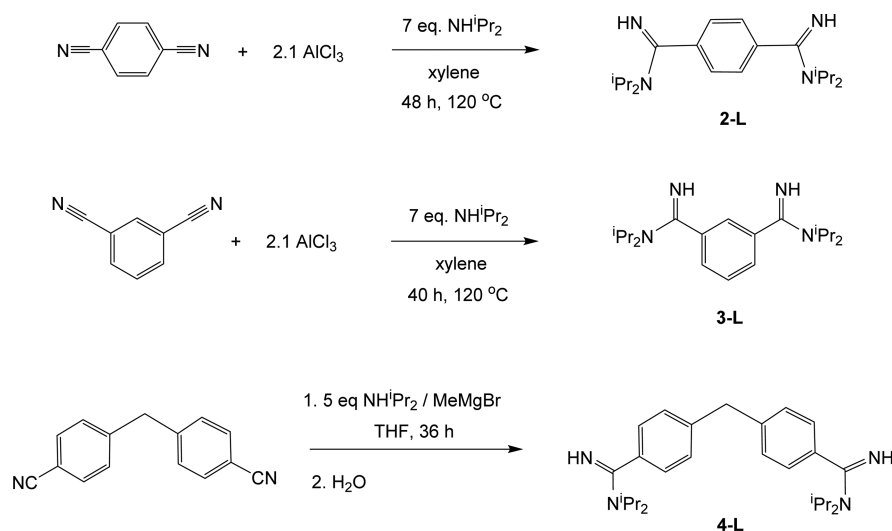
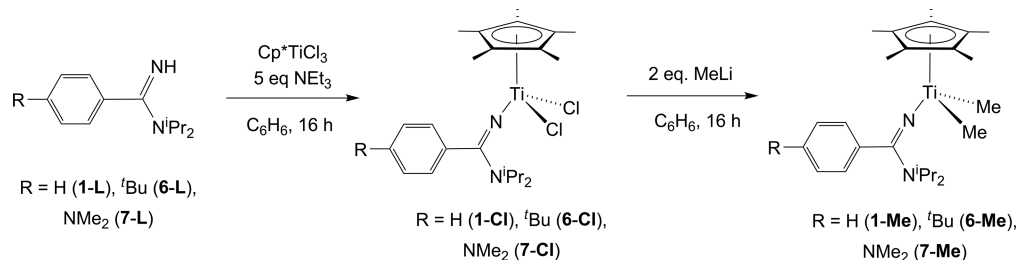
In addition to these first-developed monometallic catalysts, bimetallic systems containing metal centers either tethered

covalently through sophisticated ligand design or brought together in a template-type manner using a binuclear cocatalyst (i.e. a bis(borane) or bis(borate) species) have been reported in the last 10–15 years as delivering beneficial cooperative effects in olefin polymerization.¹⁴ Metallocene, half-sandwich, and non-cyclopentadienyl systems have all been studied. Although not all bimetallic systems show strong (or indeed any) improvements, enhancements to molecular weight capacity,¹⁵ chain branching,^{15a,16} and degree of α -olefin enchainment^{15b,16,17} as well as stereo- and regiochemistry^{15c,18} have all been demonstrated. These effects have been attributed (with computational support¹⁹ in certain cases) to secondary interactions from a proximate metal center acting on either a growing polymer chain, monomer unit, or terminated polymer chain.

Arlanxeo²⁰ has developed (as Keltan ACE)²¹ a class of half-sandwich κ^1 -amidinate titanium complexes of the type $(\eta\text{-C}_5\text{R}_5)\text{Ti}\{\text{NC}(\text{Ar})\text{NR}'_2\}\text{X}_2$ ($\text{X} = \text{Me}$ or Cl), which are extremely active precatalysts for the commercial homo- and copolymerization of olefins.^{9a–c} In a preliminary communication, we reported the synthesis and activation chemistry of

Received: March 26, 2017

Scheme 1. Synthesis of New Bis(amidine) Compounds

Scheme 2. Synthesis of Monometallic κ^1 -Amidinate Titanium Complexes

$\text{Cp}^*\text{Ti}\{\text{NC}(\text{Ar}^{\text{F}_2})\text{N}^i\text{Pr}_2\}\text{Me}_2$ ($\text{Ar}^{\text{F}_2} = \text{C}_6\text{H}_3\text{F}_2$ (9-Me)) and some preliminary results regarding the copolymerization of ethylene and propylene.^{9d} Here, we expand on our preliminary communication by evaluating a series of mono- and bimetallic complexes, their activation chemistry, and their olefin polymerization performance using borate and other activators, together with density functional theory (DFT) studies.

RESULTS AND DISCUSSION

Synthesis and Characterization of Mono- and Bimetallic κ^1 -Amidinate Titanium Complexes. *Ligand Synthesis.* The neutral benzamidinate $\text{HNC}(\text{Ph})\text{N}^i\text{Pr}_2$ (1-L) was synthesized as a ligand precursor by nucleophilic attack on the nitrile group of PhCN by the in situ generated magnesium amide, $^i\text{Pr}_2\text{NMgBr}$, followed by quenching with methanol and water. The same method was initially used to synthesize three new bis(amidine) compounds: 1,4- $\text{C}_6\text{H}_4\{\text{C}(\text{N}^i\text{Pr}_2)\text{NH}\}_2$ (2-L), 1,3- $\text{C}_6\text{H}_4\{\text{C}(\text{N}^i\text{Pr}_2)\text{NH}\}_2$ (3-L), and the unconjugated variant $\text{CH}_2\{1,4\text{-C}_6\text{H}_4\text{-C}(\text{N}^i\text{Pr}_2)\text{NH}\}_2$ (4-L). Unlike their monosubstituted and non-conjugated counterparts (e.g., 4-L), very forcing conditions were required for both 2-L and 3-L, and low yields were obtained (34–38%). A large excess of the in situ generated Grignard reagent, $^i\text{Pr}_2\text{NMgBr}$, and a prolonged reaction time (24 h) under reflux conditions in the case of 3-L were required. This is likely a result of the difficulty of a nucleophilic attack taking place on a nitrile conjugated to a deprotonated amidine. However, using AlCl₃ in the presence of an excess of diisopropylamine at high temperature (120 °C) in a minimum amount of xylene proved to be higher yielding for 2-L and 3-L (86 and 80%, respectively). The synthetic routes are summarized in Scheme 1. The synthesis

of 1,2- $\text{C}_6\text{H}_4\{\text{C}(\text{N}^i\text{Pr}_2)\text{NH}\}_2$ was not attempted due to the facile formation of phthalocyanines from the required precursors.

Synthesis of Titanium Complexes. The monometallic dichloride $\text{Cp}^*\text{Ti}\{\text{NC}(\text{Ph})\text{N}^i\text{Pr}_2\}\text{Cl}_2$ (1-Cl) was prepared in 54% yield by reaction of $\text{HNC}(\text{Ph})\text{N}^i\text{Pr}_2$ (1-L) with Cp^*TiCl_3 in the presence of an excess of triethylamine (Scheme 2). Methylation of 1-Cl with 2 equiv of MeLi proceeded smoothly to give $\text{Cp}^*\text{Ti}\{\text{NC}(\text{Ph})\text{N}^i\text{Pr}_2\}\text{Me}_2$ (1-Me) in 40% isolated yield following recrystallization from hexane.

An NMR tube scale experiment showed that 1-Me could alternatively be prepared from Cp^*TiMe_3 and 1 equiv of 1-L. This protonolysis pathway was employed for the syntheses of 1,4- $\text{C}_6\text{H}_4\{\text{C}(\text{N}^i\text{Pr}_2)\text{N}\}_2\{\text{Cp}^*\text{TiMe}_2\}_2$ (2-Me), 1,3- $\text{C}_6\text{H}_4\{\text{C}(\text{N}^i\text{Pr}_2)\text{N}\}_2\{\text{Cp}^*\text{TiMe}_2\}_2$ (3-Me), and $\text{CH}_2\{1,4\text{-C}_6\text{H}_4\text{-C}(\text{N}^i\text{Pr}_2)\text{N}\}_2\{\text{Cp}^*\text{TiMe}_2\}_2$ (4-Me) from the respective bis(amidine) in 51, 46, and 48% isolated yields, respectively (Scheme 3). The new compounds 1-Cl, 1-Me, 2-Me, 3-Me, and 4-Me were fully characterized by standard spectroscopic and analytical techniques (see the Supporting Information).

The ¹H NMR spectra (298 K, C₆D₆) of 1-Cl, 1-Me, 2-Me, 3-Me, and 4-Me indicate C_s symmetry on the NMR time scale. Broad resonances are observed for the isopropyl groups as a result of restricted rotation about the C–NⁱPr₂ bond. At low temperature, the isopropyl group signals resolve into two doublets and two septets in the case of 1-Cl, 1-Me, 2-Me, and 4-Me. The planar chirality of 3-Me results in all four methyl groups of –NⁱPr₂ becoming inequivalent, and the TiMe₂ signal decoalesces into two resonances. For the same amidinate ligand, it is invariably found that the barrier to rotation about the C–NⁱPr₂ bond is lower for the titanium dimethyl complexes than the dichloride ones, consistent with the structural data reported

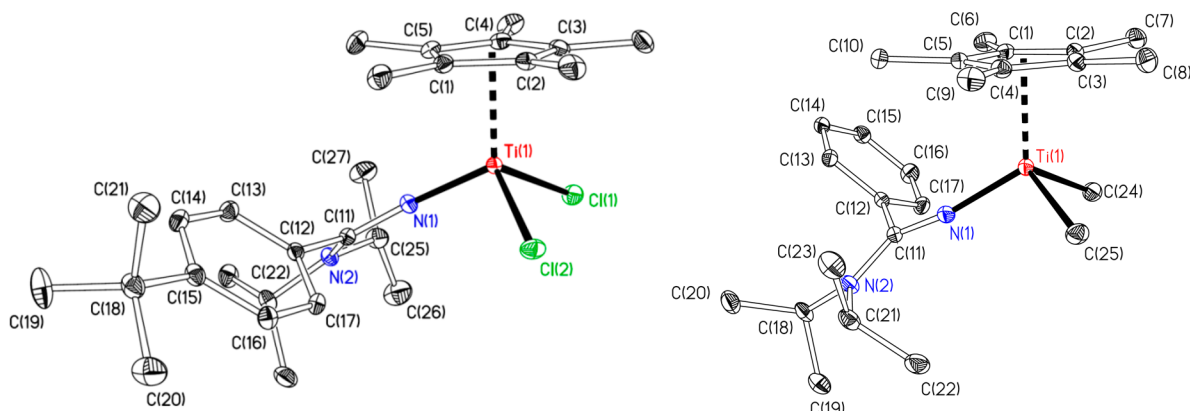
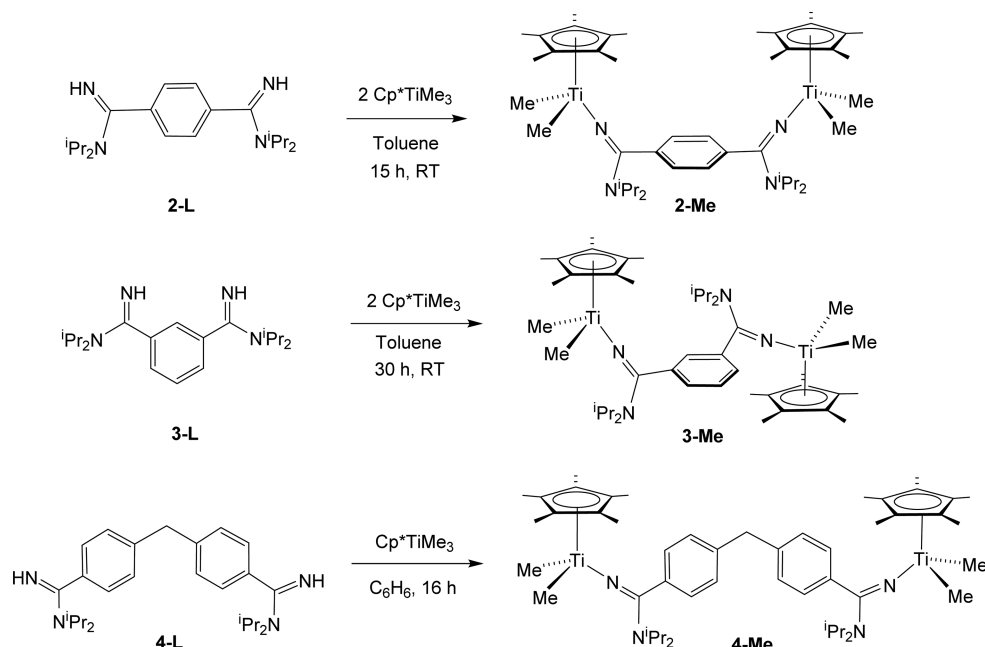
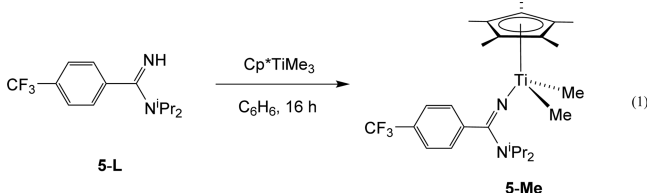
Scheme 3. Synthesis of New Bimetallic κ^1 -Amidinate Titanium Compounds

Figure 1. Displacement ellipsoid plots of $\text{Cp}^*\text{Ti}\{\text{NC}(\text{Ar}^{\text{tBu}})\text{N}^{\text{iPr}_2}\text{Cl}_2$ (**6-Cl**, left) and $\text{Cp}^*\text{Ti}\{\text{NC}(\text{Ph})\text{N}^{\text{iPr}_2}\}\text{Me}_2$ (**1-Me**, right) (20% probability; C-bound H atoms were omitted).

later (longer C–N^{iPr}₂ and shorter C=N–Ti bonds for the dimethyl complexes).



A further series of para-substituted benzamidinate complexes $\text{Cp}^*\text{Ti}\{\text{NC}(\text{Ar}^{\text{R}})\text{N}^{\text{iPr}_2}\}\text{Me}_2$ ($\text{Ar}^{\text{R}} = 4\text{-C}_6\text{H}_4\text{R}$, R = CF₃ (**5-Me**), ^tBu (**6-Me**), or NMe₂ (**7-Me**)) were also synthesized. These were prepared either directly or indirectly from the corresponding neutral analogues of **1-L**, namely, **5-L**, **6-L**, and **7-L**. The benzamidines themselves were obtained in 55–84% yield by an analogous route to that used for **1-L** (see the Supporting Information).²²

A protonolysis reaction between $\text{HNC}(\text{Ar}^{\text{CF}_3})\text{N}^{\text{iPr}_2}$ (**5-L**) and Cp^*TiMe_3 proved facile and generated $\text{Cp}^*\text{Ti}\{\text{NC}(\text{Ar}^{\text{CF}_3})\text{N}^{\text{iPr}_2}\}\text{Me}_2$ (**5-Me**) in good yield at room temperature within

17 h (eq 1). The analogous reactions of Cp^*TiMe_3 with $\text{HNC}(\text{Ar}^{\text{tBu}})\text{N}^{\text{iPr}_2}$ (**6-L**) or $\text{HNC}(\text{Ar}^{\text{NMe}_2})\text{N}^{\text{iPr}_2}$ (**7-L**) were unsuccessful even at elevated temperatures. This reduced reactivity apparently results from the more electron-donating ^tBu and NMe₂ para-substituents of **6-L** and **7-L** decreasing the acidity of the amidine (the Hammett σ_{p} values are 0.54, –0.20, and –0.83 for CF₃, ^tBu, and NMe₂, respectively, with σ_{p} for H being defined as 0.0).²³ Fortunately, reaction of **6-L** or **7-L** with Cp^*TiCl_3 in the presence of an excess of triethylamine gave the dichloride complexes $\text{Cp}^*\text{Ti}\{\text{NC}(\text{Ar}^{\text{tBu}})\text{N}^{\text{iPr}_2}\}\text{Cl}_2$ (**6-Cl**) and $\text{Cp}^*\text{Ti}\{\text{NC}(\text{Ar}^{\text{NMe}_2})\text{N}^{\text{iPr}_2}\}\text{Cl}_2$ (**7-Cl**) in 48 and 79% yields, respectively (Scheme 2). Subsequent reaction with 2 equiv of MeLi gave the target dimethyl compounds $\text{Cp}^*\text{Ti}\{\text{NC}(\text{Ar}^{\text{tBu}})\text{N}^{\text{iPr}_2}\}\text{Me}_2$ (**6-Me**) and $\text{Cp}^*\text{Ti}\{\text{NC}(\text{Ar}^{\text{NMe}_2})\text{N}^{\text{iPr}_2}\}\text{Me}_2$ (**7-Me**). The ¹H and ¹³C NMR spectra of compounds **5-Me**, **6-Me**, and **7-Me** were generally comparable to those of **1-Me** and to each other.

In addition to the amidinate ligands and complexes so far mentioned with neutral para-substituents, we attempted to prepare complexes of the type $[\text{Cp}^*\text{Ti}\{\text{NC}(\text{Ar}^{\text{R}^+})\text{N}^{\text{iPr}_2}\}\text{X}_2]\text{[BAR}^{\text{F}}_4]$ (X = Cl or Me; Ar^F = C₆F₅; Ar^{R+} = 4-C₆H₄NMe₃) as a

better mimic of the electronic effects of a distal cationic metal center in the activate bimetallic polymerization catalysts. Unfortunately, these attempts were all unsuccessful. Further details are given in the [Supporting Information](#).

Solid-State Structures of Neutral Benzamidines and Dichloride Complexes. The neutral amidines **1-L**, **2-L**, **3-L**, and **5-L** have all been crystallographically characterized. The structures and selected bond lengths and angles are given in [Figure S1](#) and [Table S1](#). The bond lengths and angles are all within the usual ranges,²⁴ and there are no significant differences between any of the structures, despite the differences in para-substituent. In all cases, the phenyl ring lies approximately perpendicular to the $\text{N}(1)=\text{C}(1)-\text{N}(2)\text{Pr}_2$ plane, presumably to avoid unfavorable steric interactions. Therefore, there is little or no π -conjugation between the $4\text{-C}_6\text{H}_4\text{R}$ ring and the $-\text{C}(\text{N}^i\text{Pr}_2)=\text{N}-\text{Ti}$ linkage.

Diffraction-quality crystals of the dichlorides $\text{Cp}^*\text{Ti}\{\text{NC}(\text{Ph})\text{N}^i\text{Pr}_2\}\text{Cl}_2$ (**1-Cl**), $\text{Cp}^*\text{Ti}\{\text{NC}(\text{Ar}^{\text{tBu}})\text{N}^i\text{Pr}_2\}\text{Cl}_2$ (**6-Cl**), and $\text{Cp}^*\text{Ti}\{\text{NC}(\text{Ar}^{\text{NMe}_2})\text{N}^i\text{Pr}_2\}\text{Cl}_2$ (**7-Cl**) were also obtained. The molecular structure of **6-Cl** is shown by way of example in [Figure 1](#), and the others are shown in [Figure S2](#). Selected bond distances and angles for all three are listed in [Table 1](#).

Table 1. Selected Bond Lengths (Å) and Angles (deg) for $\text{Cp}^*\text{Ti}\{\text{NC}(\text{Ph})\text{N}^i\text{Pr}_2\}\text{Cl}_2$ (1-Cl**), $\text{Cp}^*\text{Ti}\{\text{NC}(\text{Ar}^{\text{tBu}})\text{N}^i\text{Pr}_2\}\text{Cl}_2$ (**6-Cl**), and $\text{Cp}^*\text{Ti}\{\text{NC}(\text{Ar}^{\text{NMe}_2})\text{N}^i\text{Pr}_2\}\text{Cl}_2$ (**7-Cl**)^a**

parameter	1-Cl	6-Cl	7-Cl
Ti(1)–Cp* _{cent}	2.05	2.04	2.05
Ti(1)–N(1)	1.800(3)	1.798(2)	1.792(2)
N(1)–C(11)	1.310(4)	1.302(3)	1.310(2)
N(2)–C(11)	1.340(4)	1.355(3)	1.344(2)
C(11)–C(12)	1.509(5)	1.499(3)	1.499(3)
Ti(1)–Cl(1)	2.3137(11)	2.2965(8)	2.2927(6)
Ti(1)–Cl(2)	2.3051(11)	2.3066(7)	2.3266(6)
Cp* _{cent} –Ti(1)–N(1)	118.0	116.0	117.8
Cp* _{cent} –Ti(1)–Cl(1)	113.5	115.1	116.2
Cp* _{cent} –Ti(1)–Cl(2)	115.0	115.1	112.9
C(11)–N(1)–Ti(1)	165.2(3)	168.25(19)	164.28(14)

^aCp*_{cent} is the computed Cp* ring carbon centroid.

All of the complexes have the expected three-legged piano stool arrangement at titanium, and the Ti–Cl and Ti–Cp* distances lie within the usual ranges. The Ti(1)–N(1) bond lengths (av. 1.796, range 1.7920(17)–1.800(3) Å) are significantly longer than the typical values for a Ti–N_{amide} ($\sigma^2\pi^2$) partial double bond (typically 1.90–2.00 Å)²⁵ and are closer to those of Ti \equiv N ($\sigma^2\pi^4$) triple bonds, closer to those of the titanium amido TiN,²⁶ which usually lie in the range ca. 1.69–1.75 Å.^{24,27} They are also all significantly shorter than that in the ketimide analogue $\text{Cp}^*\text{Ti}(\text{NC}^{\text{tBu}})_2\text{Cl}_2$ (**8**; Ti–N = 1.844(7) Å).²⁸ These data suggest a Ti–N bonding description in $\text{Cp}^*\text{Ti}\{\text{NC}(\text{Ar}^{\text{R}})\text{N}^i\text{Pr}_2\}\text{Cl}_2$ that lies between the two extremes of $\sigma^2\pi^2$ (amide-like) and $\sigma^2\pi^4$ (imide-like), such that the donating capacity of the amidinate group is intermediate between the 3- and 5-electron limits (cf. resonance forms **A** and **B** in [Figure 2](#)), as has been discussed for the related phosphinimide and cyclic guanidinate counterparts.^{6b,7a} The approximately linear C(11)–N(1)–Ti(1) bond angles (av. 165.9°, range 164.28(14)–168.25(19)°) are consistent with effective π -donation from N(1). The NⁱPr₂ nitrogen N(2) and the central carbon C(11) of the ArC(N)NⁱPr₂ linkage have approximately

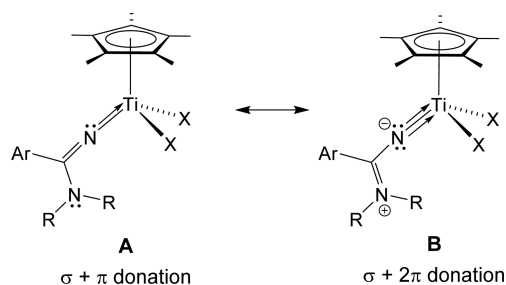


Figure 2. Resonance contributions to Ti–N_{amidinate} bonding: (A) 3-electron donor, $\sigma^2\pi^2$ Ti–N_{amidinate} bond; (B) 5-electron donor (“imide-like”) $\sigma + 2\pi$ Ti–N_{amidinate} bond.

trigonal planar geometries, implying sp^2 hybridization, and the N(2)–C(11) and C(11)–N(1) distances (av. 1.346 and 1.307 Å) are shorter and longer, respectively, than in the parent amidines themselves (av. 1.365 and 1.289 Å, respectively; cf. [Figure S1](#) and [Table S1](#)), consistent with a significant contribution from the imide-like resonance form **B** ([Figure 2](#)). The bonding is discussed in further details below.

In all three complexes, as in the neutral benzamidines themselves, the planes of the aryl ring carbons lie approximately perpendicular to the $\text{N}(1)=\text{C}(11)-\text{N}(2)\text{Pr}_2$ plane (av. rotation out of coplanarity = ca. $65 \pm 10^\circ$). As a result, even though the phenyl para-substituent varies considerably among the three compounds, there is no statistically significant change for any of the key structural parameters. Nonetheless, the Ti(1)–N(1) distance in $\text{Cp}^*\text{Ti}\{\text{NC}(\text{Ar}^{\text{NMe}_2})\text{N}^i\text{Pr}_2\}\text{Cl}_2$ (**7-Cl**), with the strongest donor para-substituent, appears to tend toward the shortest of the three examples.

Solid-State Structures of the Dimethyl Complexes. Diffraction-quality crystals of the monotitanium dimethyl compounds $\text{Cp}^*\text{Ti}\{\text{NC}(\text{Ph})\text{N}^i\text{Pr}_2\}\text{Me}_2$ (**1-Me**), $\text{Cp}^*\text{Ti}\{\text{NC}(\text{Ar}^{\text{tBu}})\text{N}^i\text{Pr}_2\}\text{Me}_2$ (**6-Me**), and $\text{Cp}^*\text{Ti}\{\text{NC}(\text{Ar}^{\text{NMe}_2})\text{N}^i\text{Pr}_2\}\text{Me}_2$ (**7-Me**) were also obtained. The molecular structure of **1-Me** is shown in [Figure 1](#) by way of example, and the others are given in [Figure S3](#). Selected distances and angles are listed in [Table 2](#). As expected, the geometries are broadly similar to those of their dichloride counterparts, with the Ti(1)–Me and Ti(1)–Cp* distances and other parameters being within the usual ranges. The Ti(1)–Cp*_{cent} (av. 2.07 Å) and Ti–N(1) distances (av. 1.845 Å) are, however, significantly lengthened compared to the dichlorides (corresponding values 2.05 and 1.797 Å, respectively) because of the superior σ -donor ability of Me compared to Cl. The lengthening of the Ti(1)–N(1) distances is accompanied by a shortening of N(1)–C(11) and lengthening of N(2)–C(11), compared to the dichlorides. Apart from these global changes on methylation, there are no significant systematic structural variations between their bond distances and angles, although, as for its dichloride counterpart, $\text{Cp}^*\text{Ti}\{\text{NC}(\text{Ar}^{\text{NMe}_2})\text{N}^i\text{Pr}_2\}\text{Me}_2$ (**7-Me**) tends toward the shortest Ti(1)–N(1) distance, but it is not within a three standard deviations difference in comparison with the corresponding values for **1-Me** and **6-Me**.

The crystallographically determined structures of the bimetallic complexes $1,4\text{-C}_6\text{H}_4\{\text{C}(\text{N}^i\text{Pr}_2)\text{N}\}_2\{\text{Cp}^*\text{TiMe}_2\}_2$ (**2-Me**) and $1,3\text{-C}_6\text{H}_4\{\text{C}(\text{N}^i\text{Pr}_2)\text{N}\}_2\{\text{Cp}^*\text{TiMe}_2\}$ are shown in [Figure 3](#), and selected bond distances and angles are listed in [Table 3](#). The solid-state structures are consistent with the variable temperature solution NMR studies described above. As expected from the 1,4- and 1,3-phenylene linkages, there are no close through-space interactions between the metal centers.

Table 2. Selected Bond Lengths (Å) and Angles (deg) for $\text{Cp}^*\text{Ti}\{\text{NC}(\text{Ph})\text{N}^i\text{Pr}_2\}\text{Me}_2$ (1-Me), $\text{Cp}^*\text{Ti}\{\text{NC}(\text{Ar}^{i\text{Bu}})\text{N}^i\text{Pr}_2\}\text{Me}_2$ (6-Me), and $\text{Cp}^*\text{Ti}\{\text{NC}(\text{Ar}^{\text{NMe}_2})\text{N}^i\text{Pr}_2\}\text{Me}_2$ (7-Me)^a

parameter	1-Me	6-Me	7-Me
Ti(1)–Cp* _{cent}	2.07	2.06	2.07
Ti(1)–N(1)	1.845(1)	1.847(2)	1.835(2)
N(1)–C(11)	1.290(2)	1.290(3)	1.297(2)
N(2)–C(11)	1.363(2)	1.357(3)	1.356(2)
C(11)–C(12)	1.502(2)	1.507(4)	1.503(2)
Ti(1)–Me(1)	2.1227(18)	2.108(3)	2.116(2)
Ti(1)–Me(2)	2.1326(19)	2.127(3)	2.1392(18)
Cp* _{cent} –Ti(1)–N(1)	120.8	120.3	119.7
Cp* _{cent} –Ti(1)–Me(1)	113.9	114.1	114.1
Cp* _{cent} –Ti(1)–Me(2)	113.9	113.3	114.4
C(11)–N(1)–Ti(1)	163.00(13)	161.1(2)	163.05(18)

^aCp*_{cent} is the computed Cp* ring carbon centroid.

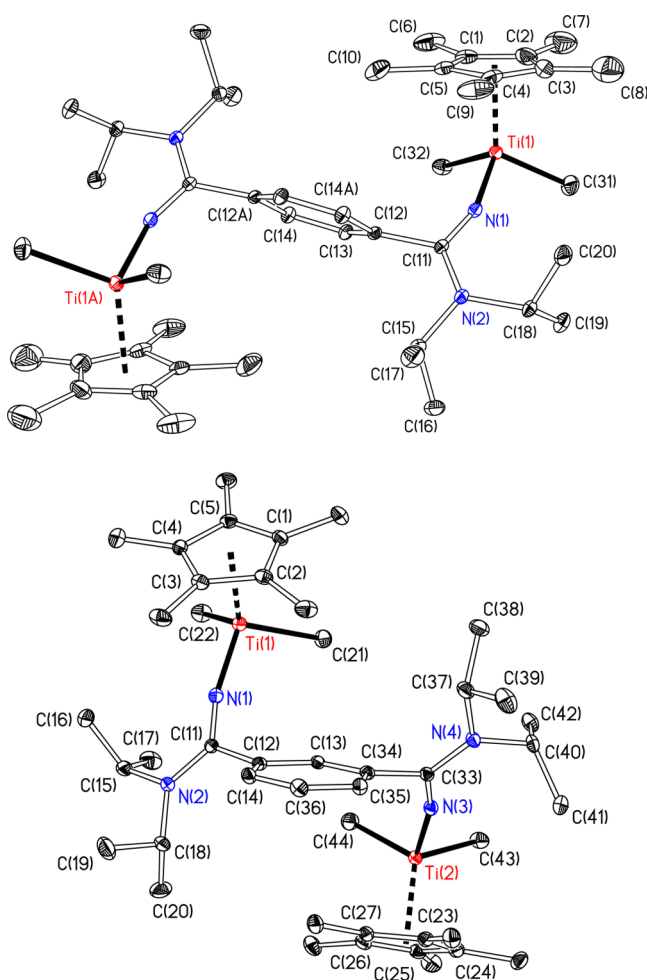


Figure 3. Displacement ellipsoid plots of $1,4\text{-C}_6\text{H}_4\{\text{C}(\text{N}^i\text{Pr}_2)\text{N}\}_2\{\text{Cp}^*\text{TiMe}_2\}_2$ (2-Me, top) and $1,3\text{-C}_6\text{H}_4\{\text{C}(\text{N}^i\text{Pr}_2)\text{N}\}_2\{\text{Cp}^*\text{TiMe}_2\}_2$ (3-Me, bottom). Atoms carrying the suffix 'A' are related to their counterparts by the symmetry operator $2 - x, 1 - y, 1 - z$.

The metal centers in 2-Me are related by crystallographic inversion symmetry, whereas those of 3-Me are independent. Comparison of the metric parameters for 2-Me and 3-Me with each other or with those of 1-Me again revealed no significant structural differences.

Table 3. Selected Bond Lengths (Å) and Angles (deg) for $1,4\text{-C}_6\text{H}_4\{\text{C}(\text{N}^i\text{Pr}_2)\text{N}\}_2\{\text{Cp}^*\text{TiMe}_2\}_2$ (2-Me) and $1,3\text{-C}_6\text{H}_4\{\text{C}(\text{N}^i\text{Pr}_2)\text{N}\}_2\{\text{Cp}^*\text{TiMe}_2\}_2$ (3-Me)^a

parameter	2-Me	3-Me	
Ti(1)–Cp* _{cent}	2.07	2.07	[2.06]
Ti(1)–N(1)	1.849(2)	1.836(2)	[1.845(2)]
N(1)–C(11)	1.285(3)	1.288(3)	[1.293(3)]
N(2)–C(11)	1.363(2)	1.368(3)	[1.364(3)]
C(11)–C(12)	1.508(3)	1.502(3)	[1.505(3)]
Ti(1)–Me(1)	2.133(3)	2.133(3)	[2.124(3)]
Ti(1)–Me(2)	2.138(3)	2.125(3)	[2.121(3)]
Cp* _{cent} –Ti(1)–N(1)	119.1	119.6	[120.5]
Cp* _{cent} –Ti(1)–Me(1)	119.1	113.9	[112.8]
Cp* _{cent} –Ti(1)–Me(2)	111.0	114.6	[114.1]
C(11)–N(1)–Ti(1)	159.64(15)	163.05(18)	[163.55(17)]

^aCp*_{cent} is the computed Cp* ring carbon centroid. For 3-Me, the values in brackets are for the corresponding parameters for Ti(2).

Spectroscopic Evaluation of Amidinate Ligand Para-Substituents. ¹³C NMR spectroscopy was used as a more sensitive probe of any effects at the titanium centers of the different benzamidinate para-substituents in the monometallic complexes 1-Me and 5-Me–7-Me and also in the para-phenylene-bridged bimetallic 2-Me by way of comparison. We have also carried out a series of DFT calculations on model compounds (see Figure 5), including computing the expected ¹³C shifts for the TiMe groups. The results are summarized in Table 4 and illustrated in Figure 4.

Table 4. Measured ¹³C NMR Chemical Shifts in C₆D₆ for the TiMe Groups in $\text{Cp}^*\text{Ti}\{\text{NC}(\text{Ar}^R)\text{N}^i\text{Pr}_2\}\text{Me}_2$ (1-Me and 5-Me–7-Me) and $1,4\text{-C}_6\text{H}_4\{\text{C}(\text{N}^i\text{Pr}_2)\text{N}\}_2\{\text{Cp}^*\text{TiMe}_2\}_2$ (2-Me) and DFT Computed Values for the Corresponding Model Compounds (See Figure 5) Expressed Relative to the Computed Value for SiMe₄

compound	Ar ^R para-substituent	Hammett σ_p parameter	measured δ TiMe (ppm)	DFT computed δ TiMe (ppm)
7-Me	NMe ₂	−0.83	46.7	52.3
6-Me	^t Bu	−0.20	47.7	53.7
1-Me	H	0.0	47.9	54.3
5-Me	CF ₃	0.54	49.0	55.5
2-Me			48.2	54.7

The data for $\text{Cp}^*\text{Ti}\{\text{NC}(\text{Ar}^R)\text{N}^i\text{Pr}_2\}\text{Me}_2$ show a strong correlation between the Hammett σ_p parameter of the phenyl para-substituent (R) and the chemical shift of TiMe, with the more electron-withdrawing $-\text{CF}_3$ group ($\sigma_p = 0.54$) giving the largest δ TiMe. The agreement between the experimental and computed ¹³C values is very good in terms of both the absolute chemical shift (relative to SiMe₄) and the trends in values. The linear fit in Figure 4 allowed the relationship $\sigma_p = 1.43 \times \delta(\text{TiMe}) - 14.2$ to be determined. Thus, the σ_p value for the $4\text{-C}_6\text{H}_4\text{C}(\text{N}^i\text{Pr}_2)\text{NCp}^*\text{TiMe}_2$ moiety in 2-Me can be estimated as 0.15, which is slightly electron-withdrawing compared to H.

The ¹³C NMR data show that although there is no clear structural effect of the para-substituent that can be determined within the precision of X-ray diffraction experiments, the titanium centers are affected to a detectable extent. As mentioned, we have probed this further using DFT calculations, as discussed in the following section.

Computational Studies of Mono- and Bimetallic Amidinate Complexes. To gain a better understanding of

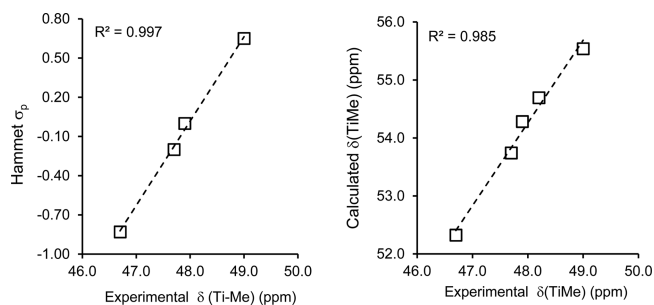


Figure 4. (Left) Relationship between the para-R-group Hammett σ_p parameter and TiMe group chemical shift in $\text{Cp}^*\text{Ti}\{\text{NC}(\text{Ar}^R)\text{N}^i\text{Pr}_2\}\text{Me}_2$. (Right) Relationship between DFT computed values for the corresponding model compounds (see Figure 5) and experimental data for $\text{Cp}^*\text{Ti}\{\text{NC}(\text{Ar}^R)\text{N}^i\text{Pr}_2\}\text{Me}_2$ and $1,4\text{-C}_6\text{H}_4\{\text{C}(\text{N}^i\text{Pr}_2)\text{N}\}_2\{\text{Cp}^*\text{TiMe}_2\}_2$ (2-Me).

the bonding in the new cyclopentadienyl-amidinate complexes described above, computational studies were carried out on a series of model and hypothetical complexes. We used a combination of DFT at the B3PW91 level and Bader's quantum theory of atoms-in-molecules (QTAIM²⁹). Because we are primarily interested in the electronic structure of the complexes and because the metal centers are similarly sterically encumbered in all of the complexes of interest, we simplified the systems by treating Cp^* as Cp and the amidinate N^iPr_2 groups as NMe_2 . To aid the reader, the numbering scheme for the computed complexes follows as closely as possible the one for the real compounds but with the suffix 'Q' appended (Figure 5). We also included the ketimide homologue $\text{CpTi}(\text{NCMe}_2)\text{Me}_2$ (8Q), a model of the real compound $\text{Cp}^*\text{Ti}(\text{NC}^i\text{Bu}_2)\text{Me}_2$ (8).^{8a} Table 5 summarizes the main computational results. Details of the calculations and Cartesian coordinates of the structures are provided in the Supporting Information.

The geometry-optimized structures of the model compounds are in good agreement with those of the real complexes. A view of the structure of 1-MeQ is shown in Figure S5, and Table 5 lists the computed Ti–N distances as a principal geometric parameter. These are systematically shorter than in the real complexes due to the reduced steric bulk, but the underlying trends reproduce those from crystallographic studies, as discussed further below. The general electronic structures of $\text{CpTi}\{\text{NC}(\text{Ar}^R)\text{NMe}_2\}\text{Me}_2$ and their homologues are in accord with the $\sigma + 2\pi$ Lewis structure depicted in Figure 2.

Molecular orbital (MO) analysis reveals two Ti–N π -bonding MOs, with further orbitals containing the Ti–N σ -bonding interaction. Key MOs for 1-MeQ are depicted by way of example in Figure S5 along with a brief discussion of their characteristics.

As mentioned, Table 5 lists the computed Ti–N distances as a principal geometric parameter in all of the compounds under consideration. For further insight into the Ti–N interactions beyond the general MO analysis, we analyzed the electron density from the DFT calculations using QTAIM.²⁹ The key QTAIM parameters here are (i) ρ_b , the electron density at the bond critical point (BCP), which can relate to bond strength within a homologous series, and (ii) the delocalization index $\delta(\text{Ti–N})$, a measure of the relative bond order within a homologous series. More generally, the positive values for the electron density Laplacian ($\Omega\nabla^2\rho_b$) and negative values for the electronic energy density (H_b) indicate covalent, donor–acceptor-like interactions between Ti and N. The ellipticity (ϵ) values show that the distribution of electron density at the Ti–N BCPs is not cylindrical, consistent with the MO analysis (non-equivalent π_h and π_v), and the description of the Ti–N bonding as formally being between forms A ($\sigma + \pi$) and B ($\sigma + 2\pi$) in Figure 3. By way of example, $\epsilon = 0$ in C_2H_2 ($\sigma^2\pi^4$) but $\epsilon > 0$ in C_2H_4 ($\sigma^2\pi^2$). $Q(\text{CpTiMe}_2)$ values are also given in Table 5. These are the formal charges on the various CpTiMe_2 fragments (i.e. the sum of the QTAIM atomic charges) and are the opposites of the charges on the NCR' ligand fragments. The values lie in the range ca. +0.4 to +0.5, reduced from $Q(\text{CpTiMe}_2) = +1.0$ for the cations $[\text{CpTiMe}_2]^+$ due to covalent interactions with the $[\text{NCR}'']^-$ anions.

The computational results show a small but systematic structural and electronic effect of varying the Ar^R group para-substituent in $\text{CpTi}\{\text{NC}(\text{Ar}^R)\text{NMe}_2\}\text{Me}_2$ from $\text{R} = \text{NMe}_2$ to CF_3 (entries 1–4, Table 5), in accordance with the ¹³C NMR trends for the real systems (Figure 4 and Table 4). The Ti–N distances lengthen from 1.827 to 1.838 Å, accompanied by the expected decrease in ρ_b and $\delta(\text{Ti–N})$ and an increase in $Q(\text{CpTiMe}_2)$, all indicating reduced $\text{N}_{\text{amidinate}} \rightarrow \text{Ti}$ donation. Figure 6 depicts the linear correlations between computed Ti–N distance and experimental Hammett σ_p (left) and $\delta(\text{Ti–N})$ (right). Examination of the energies of the σ - and two π -donor MOs for all four $[\text{NC}(\text{Ar}^R)\text{NMe}_2]^-$ anions show a general stabilization from $\text{R} = \text{NMe}_2$ to CF_3 . The computed Ti–N distances for 1-MeQ (1.833 Å) and 6-MeQ (1.834 Å) are almost equal, consistent with the crystallographic data for the real

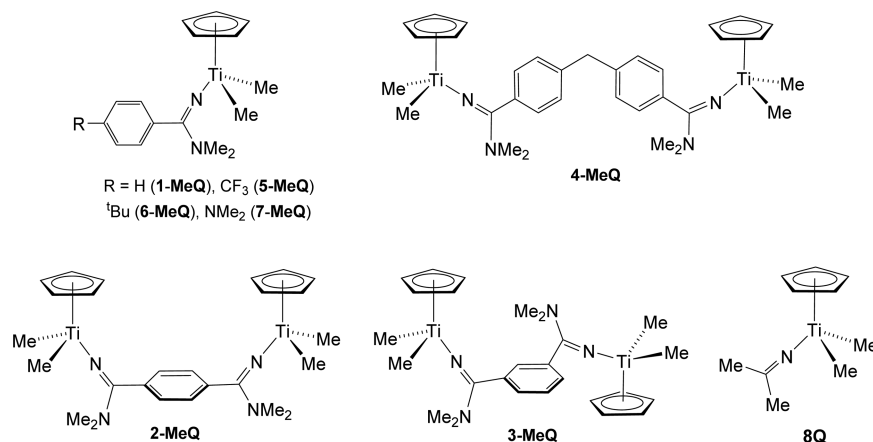


Figure 5. Neutral model complexes studied by computational methods.

Table 5. Computed Parameters for $\text{CpTi}\{\text{NC}(\text{Ar}^{\text{R}})\text{NMe}_2\}\text{Me}_2$ (**1-MeQ** and **5-MeQ-7-MeQ**), $\text{CpTi}(\text{NCMe}_2)\text{Me}_2$ (**8Q**), $1,4\text{-C}_6\text{H}_4\{\text{NCNMe}_2\}_2\{\text{CpTiMe}_2\}_2$ (**2-MeQ**), $1,3\text{-C}_6\text{H}_4\{\text{NCNMe}_2\}_2\{\text{CpTiMe}_2\}_2$ (**3-MeQ**), $\text{CH}_2\{1,4\text{-C}_6\text{H}_4\text{-C}(\text{NH})\text{NMe}_2\}_2\{\text{CpTiMe}_2\}_2$ (**4-MeQ**), and the Monomethyl Cations of the Bimetallic Species ($[\text{xQ}]^+$)^a

entry	complex	σ_p (para-R)	Ti–N (Å)	$Q(\text{CpTiMe}_2)$	ρ_b (au)	$\delta(\text{Ti–N})$	ϵ	$\nabla^2\rho_b$ (au)	H_b (au)
1	7-MeQ	−0.83 (NMe ₂)	1.827	0.413	0.145	0.964	0.214	0.580	−0.051
2	6-MeQ	−0.20 (^t Bu)	1.832	0.431	0.143	0.942	0.218	0.572	−0.049
3	1-MeQ	0 (H)	1.833	0.435	0.143	0.937	0.220	0.571	−0.049
4	5-MeQ	0.54 (CF ₃)	1.838	0.456	0.141	0.918	0.226	0.566	−0.047
5	8Q		1.856	0.475	0.135	0.892	0.383	0.548	−0.042
8	4-MeQ		1.833	0.435	0.143	0.938	0.219	0.571	−0.049
6	2-MeQ		1.834	0.443	0.142	0.934	0.230	0.575	−0.048
7	3-MeQ		1.835	0.444	0.142	0.930	0.230	0.574	−0.047
9	[2-MeQ]⁺		1.852	0.507	0.135	0.864	0.238	0.550	−0.042
10	[3-MeQ]⁺		1.845	0.493	0.137	0.892	0.246	0.563	−0.044
11	[4-MeQ]⁺		1.837	0.438	0.142	0.927	0.210	0.5644	−0.048

^aQTAIM data at the Ti–N BCPs are given in atomic units: electron density (ρ_b), electron density Laplacian ($\nabla^2\rho_b$), ellipticity (ϵ), total electronic energy density (H_b) and delocalization index ($\delta(\text{Ti–N})$).

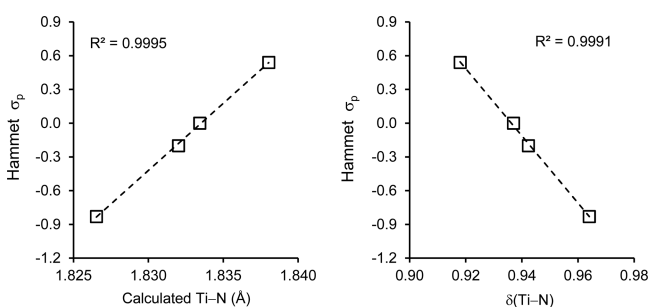


Figure 6. Relationships between the para-R-group Hammett parameter and (left) Ti–N bond distance and (right) delocalization index ($\delta(\text{Ti–N})$) in $\text{CpTi}\{\text{NC}(\text{Ar}^{\text{R}})\text{NMe}_2\}\text{Me}_2$ (R = NMe₂ (**7-MeQ**), ^tBu (**6-MeQ**), H (**1-MeQ**), or CF₃ (**5-MeQ**)).

systems (1.845(1) and 1.847(2) Å, Table 2). The computed Ti–N distance for **7-MeQ** (1.827 Å) is noticeably shorter, consistent with the shorter bond length in the real system (1.835(2) Å), although the precision in the crystallographic data did not permit a firm conclusion to be drawn within error at the $\pm 3\sigma$ level.

The computational results for the model ketimide **8Q** (entry 5) all indicate that $\text{N}_{\text{ketimide}} \rightarrow \text{Ti}$ donation is less effective than in the amidinate cases. The longer Ti–N distance for **8Q** (1.856 Å) compared to **1-MeQ** (1.833 Å) is consistent with the experimental dichloride systems $\text{Cp}^*\text{Ti}\{\text{NC}(\text{Ph})\text{N}^i\text{Pr}_2\}\text{Cl}_2$ (**1-Cl**, Ti(1)–N(1) = 1.800(3) Å) and $\text{Cp}^*\text{Ti}(\text{NC}^i\text{Bu}_2)\text{Cl}_2$ (**8**, Ti–N = 1.844(7) Å) (structural data for the relevant dimethyl compounds are not available).²⁸ The significantly increased Ti–N bond ellipticity (ϵ) for **8Q** (0.383) is consistent with the reduced role played by the more stabilized π_v MO of NCMe₂ (cf. Figure S5) in Ti–N π -bonding.

It is informative to compare the computational data for **1-MeQ** with those of the three bimetallic systems (entries 6–8). There is no significant difference between the Ti–N distances or any of the QTAIM metrics for **1-MeQ** and **4-MeQ**, the latter of which contains a $-\text{CH}_2-$ spacer group between the amidinate phenyl rings, suggesting that the methylene group “electronically insulates” the titanium centers from each other. Going from **1-MeQ** and **4-MeQ** to the 1,4- and 1,3-phenylene linked systems **2-MeQ** and **3-MeQ** leads to small but appreciable differences, consistent with the ¹³C NMR experiments for **2-MeQ**, which suggested that the para-titanium-amidinate moieties electronically influence each other by being slightly electron-withdrawing

(Table 4). Accordingly, the Ti–N distances and $Q(\text{CpTiMe}_2)$ charges in **2-MeQ** and **3-MeQ** are increased slightly compared to those in **1-MeQ** and **4-MeQ**, while the ρ_b and $\delta(\text{Ti–N})$ values are reduced.

Under olefin polymerization conditions, the mono- and bimetallic precursors are activated to cationic species of the types $[\text{Cp}^*\text{Ti}\{\text{NC}(\text{Ar}^{\text{R}})\text{NMe}_2\}\text{R}']^+$ (R = H, NMe₂, ^tBu, or CF₃) and $[(\mu\text{-L})\{\text{C}(\text{N}^i\text{Pr}_2)\text{N}\}_2\{\text{Cp}^*\text{TiR}'\}_2]^{2+}$ (L = 1,4- or 1,3-C₆H₄; (4-C₆H₄)₂CH₂), where R' represents a polymeryl chain. For the monometallic systems, the electronic nature of the para-R group does not change on activation, whereas in the bimetallic ones, each titanium will now be influenced by a neighboring cationic center. To evaluate the through-bond influence of an adjacent cationic center within the framework of the other model systems studied in Table 5, we optimized and analyzed the geometric and electronic structures of the monocationic species illustrated in Figure 7 (entries 9–11 in Table 5).

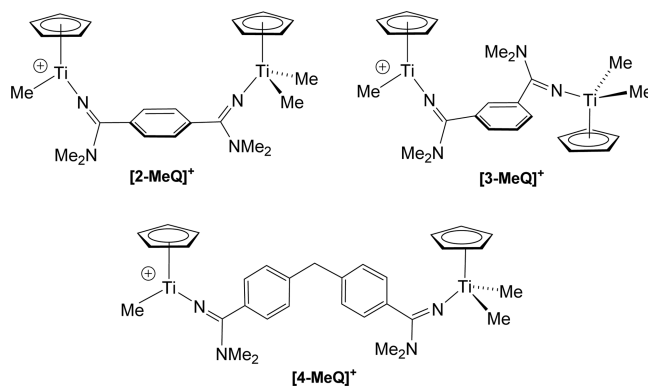


Figure 7. Cationic model complexes studied by computational methods.

The geometric and QTAIM data for **[4-MeQ]⁺** (methylene spacer, entry 11) indicate a relatively modest effect of the distal cation on the $-\text{NTiCpMe}_2$ “neutral end”. There is a small increase in $Q(\text{CpTiMe}_2)$ and Ti–N distance and a decrease in ρ_b and $\delta(\text{Ti–N})$ values. By way of comparison, we note that the magnitude of the differences between these parameters for **4-MeQ** and **[4-MeQ]⁺** is less than that between **1-MeQ** and **5-MeQ** (para-H vs para-CF₃ groups), again showing the insulating effect of the methylene spacer in this bimetallic system. In contrast, **[2-MeQ]⁺** and **[3-MeQ]⁺** show substantial

changes in the key parameters compared to those of their neutral counterparts. There are significant increases in the Ti–N distance and $Q(\text{CpTiMe}_2)$, and corresponding decreases in ρ_b and $\delta(\text{Ti–N})$. Electronically, the effect of the distal cationic titanium in $[\mathbf{2-MeQ}]^+$ and $[\mathbf{3-MeQ}]^+$ is substantially larger than that of a para- CF_3 moiety, at least as judged by the DFT results for these model systems. Finally, we note that on going from $\text{Cp}^*\text{Ti}\{\text{NC}(\text{Ar}^{\text{NMe}_2})\text{NMe}_2$ ($\mathbf{7-Me}$, entry 1), which has the most electron-releasing para-substituent, to $[\mathbf{2-MeQ}]^+$ (entry 9) there is a ca. 10% decrease in $\delta(\text{Ti–N})$ and ca. 10% increase in $Q(\text{CpTiMe}_2)$. The significance of these results with respect to polymerization performance is discussed later.

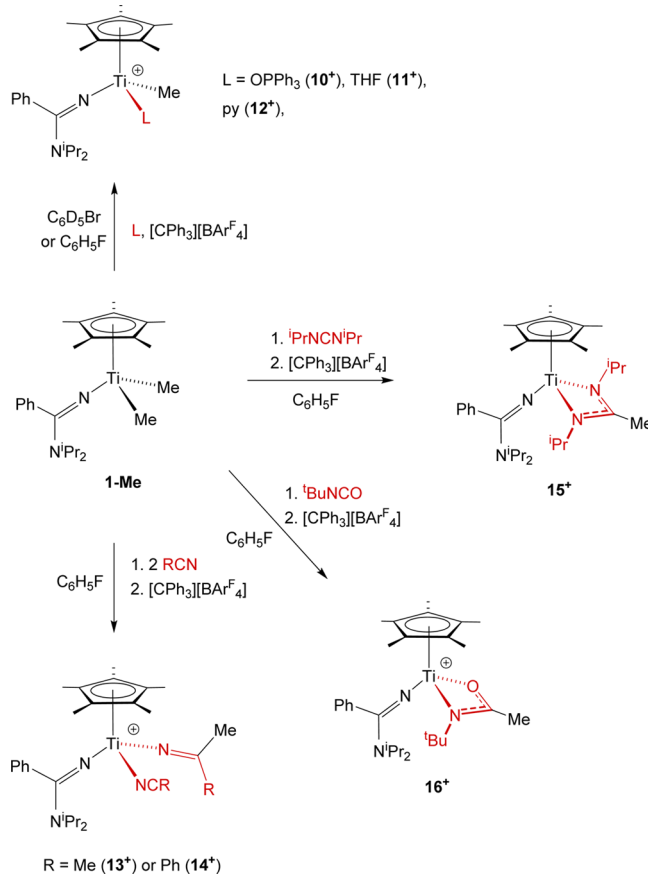
Synthesis and Stoichiometric Reactions. To better understand the activation and reactivity characteristics of representative mono- and bimetallic amidinate complexes, we carried out a number of activation and trapping reactions of cationic derivatives.

Lewis Base Adducts and Migratory Insertion Reactions. The synthesis and reactivity of Group 4 alkyl cations has been extensively investigated, especially with respect to metallocenium systems.^{15,30} Non-metallocene systems such as phosphinimide- and imido-based systems have also been studied.^{6b,12b,13,31} In a preliminary communication,^{9d} we found that $\text{Cp}^*\text{Ti}\{\text{NC}(2,6\text{-C}_6\text{H}_3\text{F}_2)\text{N}^i\text{Pr}_2\}\text{Me}_2$ ($\mathbf{9-Me}$) cleanly gave the monomethyl cation $[\text{Cp}^*\text{Ti}\{\text{NC}(2,6\text{-C}_6\text{H}_3\text{F}_2)\text{N}^i\text{Pr}_2\}\text{Me}]^+$ ($\mathbf{9}^+$) in $\text{C}_6\text{D}_5\text{Cl}$ when activated with $[\text{CPh}_3][\text{BAR}^{\text{F}_4}]$ ($\text{Ar}^{\text{F}} = \text{C}_6\text{F}_5$). Reaction of $\mathbf{9}^+$ with OPPh_3 gave the Lewis base adduct $[\text{Cp}^*\text{Ti}\{\text{NC}(2,6\text{-C}_6\text{H}_3\text{F}_2)\text{N}^i\text{Pr}_2\}\text{Me}(\text{OPPh}_3)]^+$, whereas crystallization of $\mathbf{9-BAR}^{\text{F}_4}$ afforded the unusual dimethyl-bridged dication $[\text{Cp}^*_2\text{Ti}_2\{\text{NC}(2,6\text{-C}_6\text{H}_3\text{F}_2)\text{N}^i\text{Pr}_2\}_2(\mu\text{-Me})_2]^{2+}$. No reactions with other saturated or unsaturated substrates were reported. The reactions of $\text{Cp}^*\text{Ti}\{\text{NC}(\text{Ph})\text{N}^i\text{Pr}_2\}\text{Me}_2$ ($\mathbf{1-Me}$) with Lewis bases, nitriles, and N,N' -diisopropyl carbodiimide are therefore summarized in Scheme 4. These were chosen as representative substrates based on previous chemistry for Group 4 alkyl cations.

The stoichiometric reaction of $\mathbf{1-Me}$ with $[\text{CPh}_3][\text{BAR}^{\text{F}_4}]$ in $\text{C}_6\text{D}_5\text{Br}$ on the NMR tube scale followed by addition of OPPh_3 gave immediate and quantitative formation of the Lewis base adduct $[\text{Cp}^*\text{Ti}\{\text{NC}(\text{Ph})\text{N}^i\text{Pr}_2\}(\text{OPPh}_3)\text{Me}][\text{BAR}^{\text{F}_4}]$ ($\mathbf{10-BAR}^{\text{F}_4}$), which was isolated as a yellow powder in 53% yield on scale up. In a similar way, reaction of $\mathbf{1-Me}$ with $[\text{CPh}_3][\text{BAR}^{\text{F}_4}]$ in the presence of THF or pyridine gave the corresponding adducts $[\text{Cp}^*\text{Ti}\{\text{NC}(\text{Ph})\text{N}^i\text{Pr}_2\}\text{Me}(\text{L})][\text{BAR}^{\text{F}_4}]$ ($\text{L} = \text{THF}$ ($\mathbf{11-BAR}^{\text{F}_4}$) or py ($\mathbf{12-BAR}^{\text{F}_4}$)) in 70 and 77% isolated yields, respectively. The pyridine adduct $\mathbf{12-BAR}^{\text{F}_4}$ seemed to be stable for days at RT and showed no tendency to undergo orthometalation as was found for the imido-supported cation $[(\text{Me}_3\text{TACN})\text{Ti}(\text{N}^t\text{Bu})\text{Me}]^+$ or several zirconocene alkyl cations.^{13,30c,32} Reaction of $\mathbf{1-Me}$ with the borane $\text{B}(\text{C}_6\text{F}_5)_3$ (abbreviated as BAR^{F_3}) on the NMR tube scale in $\text{C}_6\text{D}_5\text{Br}$ followed by addition of THF also formed $\mathbf{11}^+$ alongside $[\text{MeBAR}^{\text{F}_3}]^-$ as a non-coordinating anion, as discussed further below.³³

The reaction of the activated titanium complexes with nitriles formed migratory insertion products of the type found previously for metallocenium systems and $[\text{Ti}(\text{Me}_3\text{TACN})(\text{N}^t\text{Bu})\text{Me}]^+$.³⁴ Thus, reaction of $\mathbf{1-Me}$ with $[\text{CPh}_3][\text{BAR}^{\text{F}_4}]$ in the presence of 2 equiv of MeCN gave immediate formation of $[\text{Cp}^*\text{Ti}\{\text{NC}(\text{Ph})\text{N}^i\text{Pr}_2\}(\text{NCMe}_2)(\text{NCMe})][\text{BAR}^{\text{F}_4}]$ ($\mathbf{13-BAR}^{\text{F}_4}$), which was isolated in 81% yield. The analogous reaction with PhCN formed $[\text{Cp}^*\text{Ti}\{\text{NC}(\text{Ph})\text{N}^i\text{Pr}_2\}(\text{NCMePh})(\text{NCPH})][\text{BAR}^{\text{F}_4}]$ ($\mathbf{14-BAR}^{\text{F}_4}$). The rapid insertion of MeCN into the Ti–Me bond of $\mathbf{1-Me}^+$ is unlike the reaction of $[\text{Cp}_2\text{TiMe}][\text{BPh}_4]$, which takes 2 weeks to react with this substrate.^{34b,35} The insertion of nitrile

Scheme 4. Addition and Insertion Reactions of in Situ Generated Alkyl Cations with Lewis Bases and Unsaturated Substrates^a

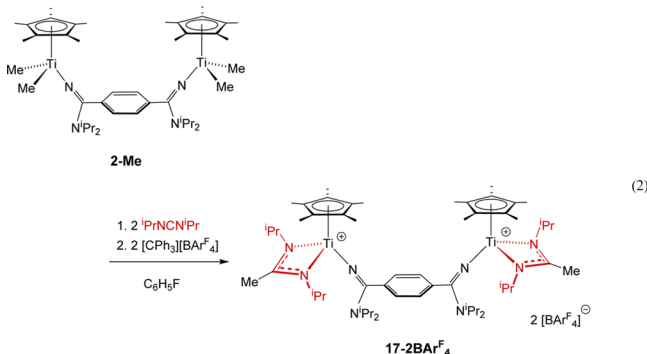


^a $[\text{BAR}^{\text{F}_4}]^-$ anions and MeCPh_3 side products were omitted for clarity.

into the Ti–Me bond as opposed to the Ti– $\text{N}_{\text{amidinate}}$ bond of $[\text{Cp}^*\text{Ti}\{\text{NC}(\text{Ph})\text{N}^i\text{Pr}_2\}\text{Me}]^+$ was established by observing ${}^1\text{H}$ – ${}^{13}\text{C}$ correlations between the migrated methyl group and the Ti– NCMePh carbon of the newly formed ketimide ligand. Further insertion reactions were carried out with N,N' -diisopropylcarbodiimide and *tert*-butylisocyanate as shown in Scheme 4. The reaction of $\mathbf{1-Me}$ with 1 equiv of N,N' -diisopropylcarbodiimide and $[\text{CPh}_3][\text{BAR}^{\text{F}_4}]$ gave $[\text{Cp}^*\text{Ti}\{\text{NC}(\text{Ph})\text{N}^i\text{Pr}_2\}\{\text{MeC}(\text{N}^i\text{Pr})_2\}][\text{BAR}^{\text{F}_4}]$ ($\mathbf{15-BAR}^{\text{F}_4}$) in very good isolated yield (77%), as did the corresponding reaction of $\mathbf{1-Me}$ with $[\text{CPh}_3][\text{BAR}^{\text{F}_4}]$ and ${}^t\text{BuNCO}$, forming $[\text{Cp}^*\text{Ti}\{\text{NC}(\text{Ph})\text{N}^i\text{Pr}_2\}\{\text{OC}(\text{Me})\text{N}^t\text{Bu}\}][\text{BAR}^{\text{F}_4}]$ ($\mathbf{16-BAR}^{\text{F}_4}$) as a red microcrystalline solid. NMR spectroscopy again confirmed that in both cases the polar heterocumulene substrate had inserted into the Ti–Me bond. Despite repeated attempts, we were unable to grow diffraction-quality crystals of an insertion product.

Activation and Trapping of Bimetallic Complexes. Corresponding activation reactions with BAR^{F_3} and $[\text{CPh}_3][\text{BAR}^{\text{F}_4}]$ were carried out for $\mathbf{2-Me}$ as a representative bimetallic analogue of $\mathbf{1-Me}$. Reaction with either 1 or 2 equiv of BAR^{F_3} or $[\text{CPh}_3][\text{BAR}^{\text{F}_4}]$ in $\text{C}_6\text{D}_5\text{Br}$ in the absence of added substrate caused a dark oil to form immediately before any NMR data could be recorded. Gratifyingly, however, in the presence of the solubilizing N,N' -diisopropylcarbodiimide, the bis(insertion) product $[\text{1,4-C}_6\text{H}_4\{\text{C}(\text{N}^i\text{Pr}_2)\text{N}\}_2\{\text{Cp}^*\text{Ti}\{\text{MeC}(\text{N}^i\text{Pr})_2\}_2\}][\text{BAR}^{\text{F}_4}]_2$ ($\mathbf{17-2BAR}^{\text{F}_4}$) was formed quantitatively on the NMR tube scale in the presence of 2 equiv of both the carbodiimide and

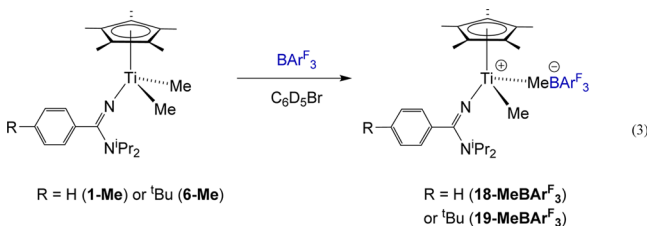
$[\text{CPh}_3][\text{BAR}^{\text{F}_4}]$. This compound was isolated in 60% yield on scale up (eq 2). The corresponding reaction using 2 equiv of



BAR^{F_3} formed the same dication on the NMR time scale along with $[\text{MeBAR}^{\text{F}_3}]^-$. The NMR and other data for 17^{2+} are analogous to those for the other insertion products and consistent with the connectivity proposed in eq 2. These experiments show that both metal centers in **2** can be activated by borate or borane and that activation of one metal center does not significantly impede activation (methyl abstraction) at the other metal center.

Probe Reactions with BAR^{F_3} . The metal centers in **1-Me** and **5-Me–7-Me** are influenced by the amidinate para-substituents, as determined by the experimental ^{13}C NMR and computational DFT/QTAIM studies described above. In an attempt to probe this further, we set out to record the ^1H and ^{19}F NMR spectra of the $[\text{Cp}^*\text{Ti}\{\text{NC}(\text{Ar}^{\text{R}})\text{N}^i\text{Pr}_2\}\{\text{MeC}(\text{N}^i\text{Pr})_2\}]^+ / [\text{MeBAR}^{\text{F}_3}]^-$ ion pairs formed on reaction of these five dimethyl compounds with BAR^{F_3} in $\text{C}_6\text{D}_5\text{Br}$ as a non-reactive/non-donor solvent. Horton et al. previously found that the separation ($\Delta_{\text{m,p}}$) of the meta and para ^{19}F chemical shifts in $[\text{MeBAR}^{\text{F}_3}]^-$ is a probe of the degree of anion association for cationic Group 4 metals. $\Delta_{\text{m,p}}$ values in the range 3–6 ppm indicate “coordination”, whereas values below 3 ppm indicate “non-coordination”.³³ We hoped that we could use $\Delta_{\text{m,p}}$ as a probe of the electronic properties of the titanium center in the activated monomethyl cations.

NMR tube scale reaction between **1-Me** and **6-Me** and BAR^{F_3} in $\text{C}_6\text{D}_5\text{Br}$ quantitatively formed single products identifiable as the ion pairs $[\text{Cp}^*\text{Ti}\{\text{NC}(\text{Ph})\text{N}^i\text{Pr}_2\}\text{Me}][\text{MeBAR}^{\text{F}_3}]$ (**18-MeBAR^F₃**) and $[\text{Cp}^*\text{Ti}\{\text{NC}(\text{Ar}^{\text{tBu}})\text{N}^i\text{Pr}_2\}\text{Me}][\text{MeBAR}^{\text{F}_3}]$ (**19-MeBAR^F₃**) (eq 3). A $\Delta_{\text{m,p}}$ value of ca. 4.7 ppm was measured



for both **18-MeBAR^F₃** and **19-MeBAR^F₃**. Although these values clearly indicate coordination of $[\text{MeBAR}^{\text{F}_3}]^-$, they also show that there is no detectable electronic differences between the titanium centers in these cations (consistent with expectation). Addition of 1 equiv of THF to **18-MeBAR^F₃** formed $[\text{Cp}^*\text{Ti}\{\text{NC}(\text{Ph})\text{N}^i\text{Pr}_2\}\text{Me}(\text{THF})][\text{MeBAR}^{\text{F}_3}]$ (**11-MeBAR^F₃**) with a $\Delta_{\text{m,p}}$ value of 2.55 ppm (indicating a noncoordinating $[\text{MeBAR}^{\text{F}_3}]^-$ anion).

Unfortunately, the analogous reactions of **5-Me** or **7-Me** (having the largest differences in ^{13}C shift for **TiMe**) with BAR^{F_3} immediately resulted in the formation of an insoluble oil. It was not possible, even under very dilute conditions, to record NMR data. To check whether cations were being formed cleanly in these two cases, carbodiimide insertion complexes of **5-Me** and **7-Me** were synthesized by adding 1 equiv of *N,N'*-diisopropylcarbodiimide prior to BAR^{F_3} , forming $[\text{Cp}^*\text{Ti}\{\text{NC}(\text{Ar}^{\text{CF}_3})\}\{\text{MeC}(\text{N}^i\text{Pr})_2\}][\text{MeBAR}^{\text{F}_3}]$ (**20-MeBAR^F₃**) and $[\text{Cp}^*\text{Ti}\{\text{NC}(\text{Ar}^{\text{NMe}_2})\}\{\text{MeC}(\text{N}^i\text{Pr})_2\}][\text{MeBAR}^{\text{F}_3}]$ (**21-MeBAR^F₃**) on the NMR tube scale.

Polymerization Studies. We have evaluated the olefin copolymerization capability of the new mono- and bimetallic titanium dimethyl complexes in conjunction with a trityl borate or a neutral borane as activator. Selected additional experiments were also performed using MAO. In our previous communication, we showed that $\text{Cp}^*\text{Ti}\{\text{NC}(\text{Ar}^{\text{F}_2})\text{N}^i\text{Pr}_2\}\text{Me}_2$ (**9-Me**) activated with $[\text{CPh}_3][\text{BAR}^{\text{F}_4}]$ is a competent catalyst (productivity = ca. $4 \times 10^4 \text{ kg mol}_{\text{Ti}}^{-1} \text{ h}^{-1} \text{ bar}^{-1}$ at 90 °C; M_n = ca. 200 kDa) for the production of an ethylene:propylene (EP) copolymer with an approximately equal $\text{C}_2:\text{C}_3$ (ethylene:propylene) content (wt %). In our current study, we were interested to extend this study of copolymerization performance to EPDM. EPDM (Figure 8) is a synthetic rubber (elastomer) formed as

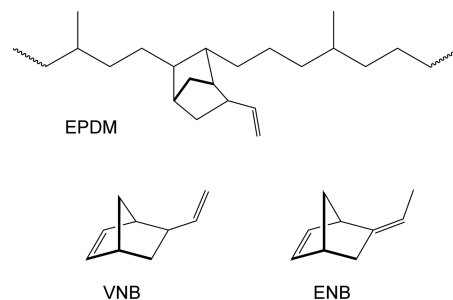


Figure 8. Representation of a segment of EPDM and the monomers VNB and ENB.

main chain saturated polymer based on the copolymerization of ethylene, propylene, and a non-conjugated diene that is incorporated into the chain in typically 2–10 wt % quantities. The diene is essential for cross-linking, which takes place post-polymerization, typically using sulfur or peroxide reagents. The dienes (Figure 8) used in this study are ENB (5-ethylidene-2-norbornene) and VNB (5-vinyl-2-norbornene), with the more strained internal double bond being incorporated into the main chain.

The polymerization results for the monomeric catalysts **1-Me** and **5-Me–7-Me** and the bimetallic systems **2-Me–4-Me** are summarized in Tables 6 and 7. Experiments were performed at 90 °C over a 10 min period (in order to avoid mass transport limitations/drift of monomer concentrations) in 1 L of pentamethylheptane as a high boiling hydrocarbon solvent in the presence of non-interacting BHT:TIBA (1:1) scavenger (BHT = 2,6-ditert-butyl-4-hydroxytoluene; TIBA = triisobutyl aluminum). A constant monomer stream of $\text{C}_2:\text{C}_3$ (1:2 molar ratio) was fed through the reactor and a large excess of ENB/VNB relative to the catalyst was introduced into the solution prior to the start of the polymerization experiment. Except where stated otherwise, the ratio of titanium center:borate or borane activator was 1:1. Hydrogen was fed into the reactor vessel along with the gaseous monomers to avoid reactor fouling caused by

Table 6. Polymerization Results for $\text{Cp}^*\text{Ti}\{\text{NC}(4\text{-C}_6\text{H}_4\text{R})\text{N}^i\text{Pr}_2\}\text{Me}_2$ ($\text{R} = \text{H}$ (1), CF_3 (5-Me), $t\text{Bu}$ (6-Me), and NMe_2 (7-Me) with $[\text{CPh}_3][\text{BAR}^F_4]$ and BAR^F_3 as Activators^a

entry	precatalyst	co-catalyst	productivity ^b (kg mol ⁻¹ h ⁻¹ bar ⁻¹)	C ₂ (wt %)	C ₃ (wt %)	ENB (wt %)	VNB (wt %)	M _n (kDa)	M _w (kDa)	PDI
1	1-Me	$[\text{CPh}_3][\text{BAR}^F_4]$	100 630	53.4	45.1	0.96	0.66	266	535	2.0
2	5-Me	$[\text{CPh}_3][\text{BAR}^F_4]$	82 800	51.1	47.1	1.10	0.74	214	454	2.1
3	6-Me	$[\text{CPh}_3][\text{BAR}^F_4]$	113 660	49.8	48.3	1.16	0.71	259	457	2.2
4	7-Me	$[\text{CPh}_3][\text{BAR}^F_4]$	80 330	54.7	43.7	0.98	0.64	210	476	2.3
5	1-Me	BAR^F_3	76 200	51.7	46.5	1.06	0.76	263	529	2.0
6	5-Me	BAR^F_3	30 170	49.6	48.6	1.07	0.74	253	547	2.2
7	6-Me	BAR^F_3	90 510	51.5	46.9	0.99	0.68	220	497	2.3
8	7-Me	BAR^F_3	53 660	55.2	42.8	1.18	0.82	251	638	2.5

^aPolymerization conditions: $T = 90$ °C, pressure = 8 bar, [catalyst] = 0.1 μmol (0.05 μmol for entry 1), scavenger = BHT:TIBA (1:1, prepared in situ, prior to precatalyst addition), $[\text{Al}]:[\text{M}] = 4500$, $[\text{B}]:[\text{Ti}] = 1:1$, 10 min reaction time, solvent = pentamethylheptane (1 L), $\text{C}_3:\text{C}_2 = 400:200$ NI h⁻¹, H_2 flow = 0.35 NI h⁻¹, ENB: 0.7 mL, VNB: 0.7 mL. Polymer molecular weight and molecular weight distributions were determined in 1,2,4-trichlorobenzene against PS standards. Average composition of the polymers was determined using transmission IR spectroscopy on a pressed polymer film. ^bProductivity per mole of transition metal centers.

Table 7. Polymerization Results for $\text{Cp}^*\text{Ti}\{\text{NC}(\text{Ph})\text{N}^i\text{Pr}_2\}\text{Me}_2$ (1), 1,4- $\text{C}_6\text{H}_4\{\text{C}(\text{N}^i\text{Pr}_2)\text{N}\}_2\{\text{Cp}^*\text{TiMe}_2\}_2$ (2-Me), 1,3- $\text{C}_6\text{H}_4\{\text{C}(\text{N}^i\text{Pr}_2)\text{N}\}_2\{\text{Cp}^*\text{TiMe}_2\}_2$ (3-Me), and $\text{CH}_2\{1,4\text{-C}_6\text{H}_4\text{-C}(\text{N}^i\text{Pr}_2)\text{N}\}_2\{\text{Cp}^*\text{TiMe}_2\}_2$ (4-Me) with $[\text{CPh}_3][\text{BAR}^F_4]$ and BAR^F_3 as Activators^a

entry	precatalyst	co-catalyst	productivity ^b (kg mol ⁻¹ h ⁻¹ bar ⁻¹)	C ₂ (wt %)	C ₃ (wt %)	ENB (wt %)	VNB (wt %)	M _n (kDa)	M _w (kDa)	PDI
1	1-Me	$[\text{CPh}_3][\text{BAR}^F_4]$	100 630	53.4	45.1	0.96	0.66	266	535	2.0
2	2-Me	$[\text{CPh}_3][\text{BAR}^F_4]$	113 910	43.6	55.3	0.68	0.43	184	399	2.2
3	3-Me	$[\text{CPh}_3][\text{BAR}^F_4]$	25 970	45.3	53.7	0.61	0.38	171	374	2.2
4	4-Me	$[\text{CPh}_3][\text{BAR}^F_4]$	132 860	50.5	47.8	0.99	0.70	227	483	2.1
5	1-Me	BAR^F_3	76 200	51.7	46.5	1.06	0.76	263	529	2.0
6	2-Me	BAR^F_3	41 310	45.4	53.5	0.66	0.45	226	465	2.1
7	3-Me	BAR^F_3	11 790	45.6	53.4	0.58	0.37	191	406	2.1
8	4-Me	BAR^F_3	43 370	52.4	46.0	0.99	0.64	218	469	2.2

^aPolymerization conditions: $T = 90$ °C, pressure = 8 bar, [catalyst] = 0.1 μmol (0.05 μmol for entries 1, 2, and 6; 0.02 μmol for entry 4), scavenger = BHT:TIBA (1:1, prepared in situ, prior to precatalyst addition), $[\text{Al}]:[\text{M}] = 4500$, $[\text{B}]:[\text{Ti}] = 1:1$, 10 min reaction time, solvent = pentamethylheptane (1 L), $\text{C}_3:\text{C}_2 = 400:200$ NI h⁻¹, H_2 flow = 0.35 NI h⁻¹, ENB: 0.7 mL, VNB: 0.7 mL. Polymer molecular weight and molecular weight distributions were determined in 1,2,4-trichlorobenzene against PS standards. Average composition of the polymers was determined using transmission IR spectroscopy on a pressed polymer film. ^bProductivity per mole of transition metal centers.

the formation of very high molecular weight EPDM.³⁶ Molecular weights (measured by GPC and expressed relative to PS standards) therefore reflect the relative rate of propagation and the rates both of chain transfer to hydrogen as well as any β -H elimination since it is known that chain transfer to aluminum with this scavenger system is negligible.³⁷ The overall weight percentages of C₂, C₃, VNB, and ENB of the EPDMs was determined by quantitative analysis of the isolated polymer films by IR spectroscopy (IR spectroscopy quantifies ENB and VNB according to their pendant double bond). The productivity values are given as kg mol⁻¹ h⁻¹ bar⁻¹ and calculated per metal center in all cases.

Monometallic Catalysts. Table 6 summarizes the polymerization results for the mononuclear catalysts $\text{Cp}^*\text{Ti}\{\text{NC}(4\text{-C}_6\text{H}_4\text{R})\text{N}^i\text{Pr}_2\}\text{Me}_2$ ($\text{R} = \text{H}$ (1), CF_3 (5-Me), $t\text{Bu}$ (6-Me), or NMe_2 (7-Me) with $[\text{CPh}_3][\text{BAR}^F_4]$ (entries 1–4) and BAR^F_3 (entries 5–8) as activators. In overall terms, the productivity and polymer composition trends (cf. Figure S6) with $[\text{CPh}_3][\text{BAR}^F_4]$ are the same as those with BAR^F_3 , showing that the same type of catalyst is formed in each case, and the PDIs (M_w/M_n) are consistent with these being well-behaved single-site catalysts. The productivities are all systematically lower with BAR^F_3 , in agreement with previous studies of these activators and the poorer coordinating ability of $[\text{BAR}^F_4]^-$ compared to $[\text{MeBAR}^F_3]^-$.^{30b,38} The general magnitude of productivities for

forming EPDM and the generally comparable C₂:C₃ ratios in the polymer are similar to the results for EP polymerization using 9-Me activated with $[\text{CPh}_3][\text{BAR}^F_4]$.^{9d} There is no systematic or significant variation in the amount of each diene (with either activator) incorporated by the different catalysts. VNB is incorporated less readily than ENB because of the differing ring strain in the monomers.

With $[\text{CPh}_3][\text{BAR}^F_4]$ as the activator, the productivity figures for 5-Me and 7-Me (entries 2 and 4) are lower than those for 1-Me and 6-Me, and this is found with BAR^F_3 also (entries 6 and 8). The reasons for this are not obvious: the para-phenyl substituents for 5-Me and 7-Me (CF_3 and NMe_2) lie at opposite ends of the range of the σ_p parameters, and all four were shown in NMR tube scale experiments (vide supra) to activate quantitatively and cleanly.

In the case of 7-Me (para- NMe_2 group) activated either with $[\text{CPh}_3][\text{BAR}^F_4]$ or BAR^F_3 , there is a small but clear reduction in propylene (C₃) affinity relative to that for ethylene (C₂) (av. wt % C₃ 43.3%) in comparison with the other catalysts. Among the other catalysts with each individual activator, there is no other clear trend, but on average, taking both activators into account, the average wt % C₃ incorporation (47.9%) for 5-Me (para- CF_3 group) is marginally the highest. There are no apparent trends for VNB/ENB content in the various polymers.

Bimetallic Catalysts. Table 7 summarizes the polymerization results for the bimetallic catalysts 1,4- $C_6H_4\{C(N^iPr_2)N\}_2\{Cp^*TiMe_2\}_2$ (**2-Me**), 1,4- $C_6H_4\{C(N^iPr_2)N\}_2\{Cp^*TiMe_2\}_2$ (**3-Me**), and $CH_2\{1,4-C_6H_4-C(N^iPr_2)N\}_2\{Cp^*TiMe_2\}_2$ (**4-Me**) and compares them with the data for the monometallic $Cp^*Ti\{NC(Ph)N^iPr_2\}Me_2$ (**1**), all with $[CPh_3][BAR^F_4]$ and BAR^F_3 activation. As found for the monometallic systems (Table 6), there is a general decrease in productivity on going from $[CPh_3][BAR^F_4]$ as activator (entries 1–4) to BAR^F_3 . In addition, the relative decrease in productivity is much larger for the bimetallic systems (entries 2–4 and 6–8, 55–67% reduction) than for **1-Me** (entries 1 and 5, 25% decrease). This may indicate a larger increase in ion pair binding between the active dication $[(\mu-L)\{Cp^*TiR'\}_2]^{2+}$ (R' = polymeryl chain, L = bis(amidinate) bridging ligand) and the more polar and “stickier” $[MeBAR^F_3]^-$ anions⁵⁹ than for the corresponding $[Cp^*Ti\{NC(Ph)N^iPr_2\}R']^+$ monocation formed from **1**.

The general trends in productivity and EPDM composition (C_2 , C_3 , diene) and molecular weights (and their associated PDIs) within the series 1–4 do not appear to change significantly with activator type. For the purposes of further discussion, we will mainly refer to the data sets in entries 1–4 with $[CPh_3][BAR^F_4]$ activation. This also minimizes effects arising from different degrees of anion coordination between the mono- and bimetallic systems.

The productivities for **1-Me** and two bimetallic systems with 1,4-substituted phenyl linkers (**2-Me**: $\mu-C_6H_4$) or (**4-Me**: $\mu-C_6H_4-CH_2-C_6H_4$) are comparable and substantially larger than for **3-Me** with a μ -1,3-phenylene linker. This may be attributed to a steric effect, which is well-precedented in the literature for bimetallic systems as metal centers are brought closer^{14a} and is also evident from the space-filling representations for **2-Me** and **3-Me** given in Figure S7. The molecular weight capability of the bimetallic systems is comparable on average with those of the monometallic ones.

The most noticeable difference between both of the $\mu-C_6H_4$ -linked bimetallics (**2-Me** and **3-Me**) and all the other catalysts studied is the change in polymer composition in terms both of higher C_3 content relative to C_2 and lower ENB/VNB content. This trend is independent of activator type: entries 2 and 3 ($[CPh_3][BAR^F_4]$) and 6 and 7 (BAR^F_3) in Table 7. This is not due to **2-Me** and **3-Me** simply being bimetallic systems per se because **4-Me** does not show this effect. **4-Me** is otherwise analogous to **2-Me** except for the 1,4- $\mu-C_6H_4-CH_2-C_6H_4$ linker in place of 1,4- $\mu-C_6H_4$, the intention being to electronically insulate the two metal centers in the active catalysts $[(\mu-L)\{Cp^*TiR'\}_2]^{2+}$. As an additional check of this result we carried out further EPDM and also ethylene-propylene (EP) polymerization experiments with **1-Me**–**4-Me** with MAO activation (Tables S2 and S3). In both cases, **2-Me** and **3-Me** have higher C_3 affinities than **1-Me** and **4-Me**, and in the case of EPDM, a lower diene content.

At first sight the clear change in polymer C_3 uptake in particular with **2-Me** and **3-Me** might be attributed to the sorts of through-space proximity effects described previously in the literature for bimetallic systems.¹⁴ However, we considered that there could alternatively (or additionally) be an electronic explanation. As discussed above in the context of the ¹³C NMR and computational studies, the electronic structure at the titanium centers in $Cp^*Ti\{NC(Ar^R)N^iPr_2\}Me_2$ are sensitive to the para-phenyl substituents in terms of Ti–N interactions (e.g., as judged by the $\delta(Ti-N)$ values) and fragment charge $Q(CpTiMe_2)$. In addition, when connected via either a 1,3- or 1,4- C_6H_4 bridge (but not a $\mu-C_6H_4-CH_2-C_6H_4$ linker), the

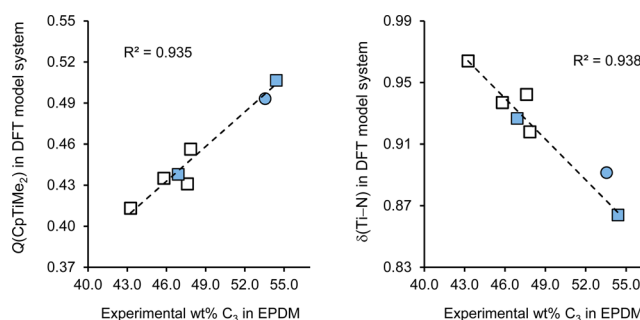


Figure 9. Relationship between experimental wt % C_3 incorporation (av. data for $[CPh_3][BAR^F_4]$ and BAR^F_3 activation) and computed (left) $Q(CpTiMe_2)$ or (right) $\delta(Ti-N)$ for the DFT model systems. Key: open squares: $Cp^R Ti\{NC(Ar^R)NR''_2\}Me_2$; filled squares: 1,4- $C_6H_4\{C(NR''_2)N\}_2\{Cp^R TiMe_2\}_2$ and $CH_2\{1,4-C_6H_4-C(NR''_2)N\}_2\{Cp^R TiMe_2\}_2$; filled circles: 1,3- $C_6H_4\{C(NR''_2)N\}_2\{Cp^R TiMe_2\}_2$. The linear regression is for the six para-substituted systems (open and filled squares). See Figure S8 and S9 for the corresponding individual plots for $[CPh_3][BAR^F_4]$ and BAR^F_3 activation. $Cp^R = Cp$ or Cp^* ; $R'' = Me$ or iPr ; $R = H, CF_3, Bu$, or NMe_2 .

charge on one titanium alkyl cation is strongly transmitted to the other one. Figure 9 explores the potential relationships between C_3 affinity for the real catalyst systems (average data for $[CPh_3][BAR^F_4]$ and BAR^F_3 activation) and the computed $Q(CpTiMe_2)$ and $\delta(Ti-N)$ electronic structure descriptors for model systems. Figures S8 and S9 give the corresponding individual plots for $[CPh_3][BAR^F_4]$ and BAR^F_3 .

As can be seen, there is an evident correlation for both the mono- and bimetallic catalyst systems between the donor ability of the amidinate moiety (as judged by the magnitude of $Q(CpTiMe_2)$ and $\delta(Ti-N)$) and C_3 affinity, with the more strongly donating amidinates (as in **7-Me**) giving the poorest α -olefin incorporation and the phenylene-linked bimetallics **2-Me** and **3-Me** having the highest. The bimetallic compound **4-Me** sits among the group of monometallic compounds with moderately donating amidinate ligands. The factors governing the α -olefin affinity in Group 4 half-sandwich catalysts are not yet clearly understood or articulated in the literature. It is known that polymerization catalysts of the type $(L)Ti(NR)Me_2$ ($L = Me_3TACN$ or related N_3 -donor) with strong $\sigma + 2\pi$ donor imido ligands have no C_3 affinity at all,^{12a,37a} whereas the titanium constrained geometry catalysts (with $\sigma + 1\pi$ donor amide ligands) have very high α -olefin affinity.³ Cyclopentadienyl-phosphinimide and -ketimide with $\sigma + 2\pi$ donor-like properties have intermediate C_3 affinities. For example, $Cp^*Ti\{NC^tBu\}Me_2$ (**8**) produces EP copolymer with 67 wt % C_3 content under the same conditions as those used for **1-Me**–**4-Me** (see Table S3).

On the basis of the tightly focused series of cyclopentadienyl-amidinate compounds described here, we find a correlation based on electronic factors between amidinate ligand donor ability and C_3 affinity. However, there is no observable correlation between diene (individual or total) content and any of the electronic descriptors within the monometallic systems. One reason for this may be the difficulty in detecting small variations when the baseline wt % incorporation of these monomers is relatively low in any case (<2%). The sterically more encumbered **2-Me** and **3-Me** systems show an unusually low affinity, with that for **3-Me** being the lowest on average. It seems that the most likely explanation here is that these more sterically demanding dienes are the most sensitive to the

increased steric crowding in **2-Me** and **3-Me** (cf. the space-filling representations in Figure S7).

SUMMARY AND CONCLUSIONS

Straightforward synthesis of the benzamidines $\text{HNC}(\text{Ar}^R)\text{N}^i\text{Pr}_2$ ($R = \text{H}$, CF_3 , ^iBu , and NMe_2) has allowed us to explore the influence of the para- R group on the solid-state structures, electronic properties at titanium, and polymerization performance of the corresponding titanium complexes $\text{Cp}^*\text{Ti}\{\text{NC}(\text{Ar}^R)\text{N}^i\text{Pr}_2\}_2\text{Me}_2$ ($R = \text{H}$ (**1**), CF_3 (**5-Me**), ^iBu (**6-Me**), or NMe_2 (**7-Me**)). ^{13}C NMR data together with detailed DFT and QAIM studies show a small but significant electronic effect at the metal center, with the donor ability of the ligands increasing with decreasing Hammett σ_p parameter in the order $R = \text{CF}_3 < \text{H} < ^i\text{Bu} < \text{NMe}_2$. The amidinate ligands are best thought of as intermediate between 3-electron ($\sigma + \pi$) and 5-electron ($\sigma + 2\pi$) donors, with a larger π -donation contribution than found in the analogous ketimide systems. Use of bis(amidine) protio-ligands gave access to the corresponding bimetallic derivatives $1,4\text{-C}_6\text{H}_4\{\text{C}(\text{N}^i\text{Pr}_2)\text{N}\}_2\{\text{Cp}^*\text{TiMe}_2\}_2$ (**2-Me**), $1,3\text{-C}_6\text{H}_4\{\text{C}(\text{N}^i\text{Pr}_2)\text{N}\}_2\{\text{Cp}^*\text{TiMe}_2\}_2$ (**3-Me**), and $\text{CH}_2\{1,4\text{-C}_6\text{H}_4\text{-C}(\text{N}^i\text{Pr}_2)\text{N}\}_2\{\text{Cp}^*\text{TiMe}_2\}_2$ (**4-Me**), which were structurally characterized for **2** and **3**. Computational studies found that the metal centers in **2-Me** and **3-Me** responded significantly to changes in charge, whereas those in **4-Me** were much better insulated from each other.

Activation reaction of **1** with $[\text{CPh}_3][\text{BAR}^F_4]$ led to cationic Lewis base adducts with OPPh_3 , THF, and pyridine and Ti–Me bond insertion products with the polar substrates MeCN, $^i\text{BuNCO}$, and $^i\text{PrNCN}^i\text{Pr}$. Although nitriles, isocyanates, and carbodiimides are susceptible to nucleophilic attack by anionic nitrogen groups, in these amidinate-supported systems the site of reactivity was invariably the TiMe group. Reaction of **1** and certain homologues with BAR^F_3 formed soluble inner-sphere ion pairs of the type $[\text{Cp}^*\text{Ti}\{\text{NC}(\text{Ar}^R)\text{N}^i\text{Pr}_2\}\text{Me}][\text{MeBAR}^F_3]$ containing coordinating $[\text{MeBAR}^F_3]^-$ anions which were displaced by THF or $^i\text{PrNCN}^i\text{Pr}$, forming Lewis base adducts or insertion products. Reaction of the bimetallic analogue **2** with 2 equiv of $[\text{CPh}_3][\text{BAR}^F_4]$ in the presence of certain trapping reagents showed that both metal centers can be readily activated. All of the mono- and bimetallic complexes were very active at 90 °C for the copolymerization of ethylene, propylene, and VNB/ENB for forming EPDM with molecular weights in the range ca. 180–280 kDa at $\text{C}_2:\text{C}_3$ ratios between ca. 57:43 and 51:49 and around 1% ENB and 0.7% VNB. For the mono-metallic systems $\text{Cp}^*\text{Ti}\{\text{NC}(\text{Ar}^R)\text{N}^i\text{Pr}_2\}_2\text{Me}_2$ activated with $[\text{CPh}_3][\text{BAR}^F_4]$ or BAR^F_3 , there was a weak influence of the para- R group on the polymer composition such that a slightly lower C_3 incorporation was found for $R = \text{NMe}_2$ and a marginally higher C_3 content for $R = \text{CF}_3$. There was no effect on diene incorporation. Analogous results were found for the bimetallic catalyst $\text{CH}_2\{1,4\text{-C}_6\text{H}_4\text{-C}(\text{N}^i\text{Pr}_2)\text{N}\}_2\{\text{Cp}^*\text{TiMe}_2\}_2$ (**4-Me**). In contrast, for **2-Me** and **3-Me** a more significant increase in C_3 affinity and decrease in diene content were observed regardless of the activator used (borate/borane and MAO). The variation in C_3 content across the mono- and bimetallic catalysts could be correlated with electronic descriptors of the donor ability of the amidinate groups (net charge $Q(\text{Cp}^*\text{TiMe}_2)$ or delocalization index ($\delta(\text{Ti}-\text{N})$) in model systems.

The lower diene uptake for **2-Me** and **3-Me** could be attributed to higher steric crowding in the phenylene-bridged systems, indicating the importance of proximity effects in

these cases. In addition, although the combined computation and experimental data point to an explanation of increased C_3 affinity based on electronic factors, the results do not exclude the possibility of additional cooperative effects in **2-Me** and **3-Me** of the types reported for other closely positioned bimetallic systems.

EXPERIMENTAL SECTION

General Methods and Instrumentation. All manipulations were carried out using standard Schlenk line or drybox techniques under an atmosphere of argon or dinitrogen. Solvents were degassed by sparging with dinitrogen and dried by passing through a column of the appropriate drying agent⁴⁰ or refluxed over sodium (toluene, xylene), potassium (THF), Na/K (Et₂O), or P₂O₅ (fluorobenzene) and distilled. Deuterated solvents were dried over sodium (C₆D₆ and toluene-*d*₈), potassium (THF-*d*₆), P₂O₅ (CDCl₃ and CD₂Cl₂), or CaH₂ (C₆D₅Br) distilled under reduced pressure and stored under argon in Teflon valve ampoules. NMR samples were prepared under dinitrogen in 5 mm Wilmad 507-PP tubes fitted with J. Young Teflon valves. ¹H, ¹³C–{¹H}, ¹¹B, and ¹⁹F NMR spectra were recorded on a Varian Mercury-VX 300, Bruker Avance 400, Bruker Avance III 500 NMR, or Bruker AVX 500 spectrometer fitted with a ¹³C cryoprobe. Spectra are referenced internally to residual protio-solvent (¹H) or solvent (¹³C) resonances and are reported relative to tetramethylsilane ($\delta = 0$ ppm). ¹⁹F spectra were referenced externally to CFCl₃, and ¹¹B spectra were referenced externally to Et₂O·BF₃. Assignments were confirmed using two-dimensional ¹H–¹H and ¹³C–¹H NMR correlation experiments. Chemical shifts are quoted in δ (ppm), and coupling constants, in Hz. Mass spectra were recorded by the mass spectrometry service of the University of Oxford. IR spectra were recorded on a Thermo Scientific Nicolet iS5 FTIR spectrometer. Samples were prepared in a drybox as Nujol mulls between NaCl plates or as a thin film, and the data are quoted in wavenumbers (cm⁻¹) within the range 4000–400 cm⁻¹. Elemental analyses were carried out by the Elemental Analysis Service at the London Metropolitan University.

Representative syntheses are given below. Further details given in the Supporting Information on the syntheses and characterization of $\text{HNC}(\text{Ph})\text{N}^i\text{Pr}_2$ (**1-L**), $1,4\text{-C}_6\text{H}_4\{\text{C}(\text{N}^i\text{Pr}_2)\text{NH}\}_2$ (**2-L**), $1,3\text{-C}_6\text{H}_4\{\text{C}(\text{N}^i\text{Pr}_2)\text{NH}\}_2$ (**3-L**), $\text{CH}_2\{1,4\text{-C}_6\text{H}_4\text{-C}(\text{N}^i\text{Pr}_2)\text{NH}\}_2$ (**4-L**), $\text{HNC}(\text{Ar}^{\text{CF}_3})\text{N}^i\text{Pr}_2$ (**5-L**), $\text{HNC}(\text{Ar}^{\text{Bu}})\text{N}^i\text{Pr}_2$ (**6-L**), $\text{HNC}(\text{Ar}^{\text{NMe}_2})\text{N}^i\text{Pr}_2$ (**7-L**), $\text{Cp}^*\text{Ti}\{\text{NC}(\text{Ph})\text{N}^i\text{Pr}_2\}_2\text{Cl}_2$ (**1-Cl**), $1,3\text{-C}_6\text{H}_4\{\text{C}(\text{N}^i\text{Pr}_2)\text{-N}\}_2\{\text{Cp}^*\text{TiMe}_2\}_2$ (**3-Me**), $\text{CH}_2\{1,4\text{-C}_6\text{H}_4\text{-C}(\text{NH})\text{N}^i\text{Pr}_2\}_2\{\text{Cp}^*\text{TiMe}_2\}_2$ (**4-Me**), $\text{Cp}^*\text{Ti}\{\text{NC}(\text{Ar}^{\text{CF}_3})\text{N}^i\text{Pr}_2\}_2\text{Me}_2$ (**5-Me**), $\text{Cp}^*\text{Ti}\{\text{NC}(\text{Ar}^{\text{Bu}})\text{-N}^i\text{Pr}_2\}_2\text{Cl}_2$ (**6-Cl**), $\text{Cp}^*\text{Ti}\{\text{NC}(\text{Ar}^{\text{Bu}})\text{N}^i\text{Pr}_2\}_2\text{Me}_2$ (**6-Me**), $\text{Cp}^*\text{Ti}\{\text{NC}(\text{Ar}^{\text{NMe}_2})\text{N}^i\text{Pr}_2\}_2\text{Cl}_2$ (**7-Cl**), $\text{Cp}^*\text{Ti}\{\text{NC}(\text{Ar}^{\text{NMe}_2})\text{N}^i\text{Pr}_2\}_2\text{Me}_2$ (**7-Me**), $[\text{Cp}^*\text{Ti}\{\text{NC}(\text{N}^i\text{Pr}_2)\text{Ph}\}\{\text{OPPh}_3\}\text{Me}][\text{BAR}^F_4]$ (**10-BAR^F₄**), $[\text{Cp}^*\text{Ti}\{\text{NC}(\text{N}^i\text{Pr}_2)\text{-Ph}\}\{\text{py}\}\text{Me}][\text{BAR}^F_4]$ (**12-BAR^F₄**), $[\text{Cp}^*\text{Ti}\{\text{NC}(\text{N}^i\text{Pr}_2)\text{Ph}\}\{\text{NCMe}_2\}\text{-}(\text{NCMe})][\text{BAR}^F_4]$ (**13-BAR^F₄**), $[\text{Cp}^*\text{Ti}\{\text{NC}(\text{N}^i\text{Pr}_2)\text{Ph}\}\{\text{NCMePh}\}\text{-}(\text{NCPh})][\text{BAR}^F_4]$ (**14-BAR^F₄**), $[\text{Cp}^*\text{Ti}\{\text{NC}(\text{Ph})\text{N}^i\text{Pr}_2\}_2\{\text{OC}(\text{Me})\text{-N}^i\text{Bu}\}][\text{BAR}^F_4]$ (**16-BAR^F₄**), $[1,4\text{-C}_6\text{H}_4\{\text{C}(\text{N}^i\text{Pr}_2)\text{N}\}_2\{\text{Cp}^*\text{Ti}\{\text{MeC}(\text{N}^i\text{Pr}_2)\}_2][\text{BAR}^F_4]$ (**17-2BAR^F₄**) and $[1,4\text{-C}_6\text{H}_4\{\text{CN}(\text{NMe}_3)\}_2]\text{Cl}$, $[1,4\text{-C}_6\text{H}_4\{\text{CN}(\text{NMe}_3)\}_2][\text{BAR}^F_4]$ (**22**); NMR time scale syntheses of $[\text{Cp}^*\text{Ti}\{\text{NC}(\text{N}^i\text{Pr}_2)\text{Ph}\}\{\text{THF}\}\text{Me}][\text{MeBAR}^F_3]$ (**11-MeBAR^F₃**), $[\text{Cp}^*\text{Ti}\{\text{NC}(\text{N}^i\text{Pr}_2)\text{Ph}\}\{\text{MeC}(\text{N}^i\text{Pr}_2)\}_2][\text{MeBAR}^F_3]$ (**15-MeBAR^F₃**), $[1,4\text{-C}_6\text{H}_4\{\text{C}(\text{N}^i\text{Pr}_2)\text{N}\}_2\{\text{Cp}^*\text{Ti}\{\text{MeC}(\text{N}^i\text{Pr}_2)\}_2][\text{MeBAR}^F_3]$ (**17-2MeBAR^F₃**), $[\text{Cp}^*\text{Ti}\{\text{NC}(\text{Ph})\text{N}^i\text{Pr}_2\}\text{Me}][\text{MeBAR}^F_3]$ (**18-MeBAR^F₃**), $[\text{Cp}^*\text{Ti}\{\text{NC}(\text{Ar}^{\text{Bu}})\text{N}^i\text{Pr}_2\}\text{Me}][\text{MeBAR}^F_3]$ (**19-MeBAR^F₃**), $[\text{Cp}^*\text{Ti}\{\text{NC}(\text{Ar}^{\text{CF}_3})\}\text{-}(\text{MeC}(\text{N}^i\text{Pr}_2))][\text{MeBAR}^F_3]$ (**20-MeBAR^F₃**), and $[\text{Cp}^*\text{Ti}\{\text{NC}(\text{Ar}^{\text{NMe}_2})\}\text{-}(\text{MeC}(\text{N}^i\text{Pr}_2))][\text{MeBAR}^F_3]$ (**21-MeBAR^F₃**).

$\text{Cp}^*\text{Ti}\{\text{NC}(\text{Ph})\text{N}^i\text{Pr}_2\}_2\text{Me}_2$ (**1-Me**). To a stirring toluene (15 mL) solution of $\text{Cp}^*\text{Ti}\{\text{NC}(\text{Ph})\text{N}^i\text{Pr}_2\}_2\text{Cl}_2$ (**1-Cl**) (1 g, 2.2 mmol) was added dropwise MeLi (2.7 mL, 1.6 M in Et₂O, 2.2 mmol), and the resulting solution was stirred for 16 h. The volatiles were then removed in vacuo, and the yellow solid was then extracted into *n*-hexanes (50 mL). Concentration of the solution to ca. 15 mL and subsequent storage at –30 °C for 24 h resulted in crystallization of the desired product as large yellow crystals, which were isolated and dried in vacuo. Yield: 0.37 g (40%). ¹H NMR (toluene-*d*₈, 299.9 MHz, 233 K): 7.23–6.95

(5 H, series of overlapping multiplets, C₆H₅), 3.60 (1 H, sept, CHMe₂ cis to C₆H₅, ³J = 6 Hz), 2.91 (1 H, br s, CHMe₂ trans to C₆H₅), 1.83 (15 H, s, C₅Me₃), 1.72 (6 H, d, CHMe₂ trans to C₆H₅, ³J = 6 Hz), 0.64 (6 H, d, CHMe₂ cis to C₆H₅, ³J = 6 Hz), 0.53 (6 H, s, Me) ppm. ¹³C-{¹H} NMR (toluene-d₆, 233 K): 160.9 (NC(Ph)NⁱPr₂), 141.9 (i-C₆H₅), 128.1 (o- or m-C₆H₅), 127.5 (m- or o-C₆H₅), 126.1 (p-C₆H₅), 118.9 (C₅Me₃), 51.7 (CHMe₂ cis to C₆H₅), 47.6 (TiMe), 46.5 (CHMe₂ trans to C₆H₅), 19.9 (CHMe₂), 11.7 (C₅Me₃) ppm. IR (NaCl plates, Nujol mull, cm⁻¹): 1563 (s), 1506 (w), 1323 (s), 1261 (w), 1132 (w), 1094 (w), 1034 (m), 1023 (m), 886 (m), 782 (s), 696 (m), 666 (m). Anal. found (calcd. for C₂₅H₄₀N₂Ti₁): C, 71.90 (72.10); H, 9.80 (9.68); N, 6.80 (6.73)%. EI-MS *m/z*: 203 (5%, [NC(Ph)NⁱPr₂]⁺), 135 (5%, [Cp*]⁺), 103 (100%, [NCPh]⁺), 77 (70%, [Ph]⁺). Single crystals suitable for X-ray diffraction were grown from a pentane solution at -30 °C.

1,4-C₆H₄(C(NⁱPr₂)N)₂(Cp*TiMe₂)₂ (2-Me). To a stirring toluene (15 mL) solution of 1,4-C₆H₄(C(NH)NⁱPr₂)₂ (1.01 g, 3.06 mmol) was added a toluene (10 mL) solution of Cp*TiMe₃ (1.46 g, 6.40 mmol). The brown solution was stirred for 15 h until a precipitate appeared. After filtration, the solid was washed with toluene (3 × 15 mL) to produce a yellow solid, which was isolated and dried in vacuo. Yield: 1.18 g (51%) Diffraction-quality crystals were grown by slow cooling from a concentrated solution of hot bromobenzene. ¹H NMR (CDCl₃, 299.9 MHz, 223 K): 7.13 (4H, s, Ar), 3.71 (2H, sept, ³J = 6.9 Hz, N(CHMe₂)₂), 3.51 (2H, br, N(CHMe₂)₂), 1.67 (12H, d, ³J = 6.6 Hz, N(CHMe₂)₂), 1.64 (30H, s, C₅Me₃), 1.39 (12H, d, ³J = 6.6 Hz, N(CHMe₂)₂), -0.19 (12H, s, TiMe₂) ppm. ¹³C-{¹H} NMR (CDCl₃, 75.4 MHz, 223 K): 160.6 (CN(NⁱPr₂)), 140.2 (Ar C(C(NⁱPr₂)N)), 125.5 (Ar CHC(C(NMe₂)N)), 118.9 (C₅Me₃), 51.8 (N(CHMe₂)₂), 46.6 (N(CHMe₂)₂), 45.9 (TiMe₂), 20.8 (N(CHMe₂)₂), 19.9 (N(CHMe₂)₂), 11.3 (C₅Me₃) ppm. IR (NaCl plates, Nujol mull, cm⁻¹): 1561 (s, C=N), 1321 (m), 1135 (w), 890 (m), 829 (w). EI-MS: *m/z* = 694 (3%, [M - 4Me]⁺). Anal. found (calcd. for C₄₄H₇₄N₄Ti₂): C, 69.85 (70.01); H, 9.68 (9.88); N, 7.57 (7.42)%.

[Cp*Ti{NC(NⁱPr₂)Ph}(THF)Me][BAR^F₄] (11-BAR^F₄). Cp*Ti{NC(NⁱPr₂)Ph}Me₂ (100 mg, 0.24 mmol) and THF (17 mg, 19 μL, 0.24 mmol) were mixed together in fluorobenzene (10 mL). To this was added a solution of [CPh₃][BAR^F₄] (221 mg, 0.24 mmol) in fluorobenzene (5 mL). After 30 min, pentane (20 mL) was added, resulting in the formation of an orange oil. The pentane/fluorobenzene was decanted away, and the oil washed further with pentane (10 mL). The remaining solvent was removed in vacuo, yielding the product as a yellow solid. Yield: 193 mg (70%). ¹H NMR (C₆D₅Br, 299.9 MHz, 293 K): 7.20–6.70 (5H, m, C₆H₅), 3.47 (1H, br, NCHMe₂), 3.39 (1H, sept, ³J = 6.8 Hz, NCHMe₂), 3.29 (2H, m, OCH₂), 3.18 (2H, m, OCH₂), 1.54 (15H, s, C₅Me₃), 1.41 (4H, m, OCH₂CH₂), 1.23 (1H, d, ³J = 6.8 Hz, NCHMe₂), 1.10 (1H, d, ³J = 6.8 Hz, NCHMe₂), 0.73 (2H, d, ³J = 6.6 Hz, NCHMe₂), 0.51 (3H, s, TiMe) ppm. ¹³C-{¹H} NMR (C₆D₅Br, 75.4 MHz, 293 K): 167.6 (NC(NⁱPr₂)Ph), 148.9 (br d, ¹J_{CF} = 244.4 Hz, o-C₆F₅), 138.6 (br d, ¹J_{CF} = 247.8 Hz, p-C₆F₅), 137.7 (i-C₆H₅), 136.8 (br d, ¹J_{CF} = 249.0 Hz, m-C₆F₅), 129.5 (o-C₆H₅), 128.9 (m-C₆H₅), 125.6 (C₅Me₃), 75.1 (OCH₂CH₂), 58.8 (Ti-Me), 52.3 (NCHMe₂), 48.5 (NCHMe₂), 25.2 (OCH₂CH₂), 21.5 (NCHMe₂), 21.0 (NCHMe₂), 20.5 (NCHMe₂), 19.8 (NCHMe₂), 11.7 (C₅Me₃) ppm. ¹⁹F NMR (C₆D₅Br, 282.1 MHz, 293 K): -131.5 (m, o-C₆F₅), -161.9 (m, p-C₆F₅), -165.8 (m, m-C₆F₅) ppm. ¹¹B NMR (C₆D₅Br, 96.2 MHz, 293 K): -15.9 ppm. IR (NaCl plates, Nujol mull, cm⁻¹): 1643 (m), 1595 (w), 1514 (s), 1345 (w), 1261 (w), 1153 (w), 1086 (m), 1023 (w), 980 (s), 891 (w), 844 (w), 789 (w), 775 (w), 756 (w), 668 (w). Anal. Found (calcd. for C₃₂H₄₅B F₂₀N₂O₂Ti): C, 53.98 (54.19); H, 3.90 (3.94); N, 2.56 (2.43)%.

[Cp*Ti{NC(NⁱPr₂)Ph}{MeC(NⁱPr₂)}][BAR^F₄] (15-BAR^F₄). Cp*Ti{NC(NⁱPr₂)Ph}Me₂ (100 mg, 0.24 mmol) and ⁱPrNCNⁱPr (30 mg, 37 μL, 0.24 mmol) were mixed together in fluorobenzene (10 mL). To this was added a solution of [CPh₃][BAR^F₄] (221 mg, 0.24 mmol) in fluorobenzene (5 mL). After 30 min, pentane (20 mL) was added, resulting in the formation of a brown solid. The pentane/fluorobenzene was decanted away, and the solid washed further with pentane (10 mL). The solid was dried in vacuo, yielding the product as a brown solid. Yield: 220 mg (77%). ¹H NMR (CD₂Cl₂, 299.9 MHz, 293 K): 7.50–7.20 (5H, m, C₆H₅), 4.21 (1H, br, κ¹-NCHMe₂), 3.67 (3H, overlapping sept,

κ¹- and κ²-NCHMe₂), 2.28 (1H, s, MeC(NⁱPr₂)), 2.08 (15H, s, C₅Me₃), 1.40 (6H, d, ³J = 6.9 Hz, κ¹-NCHMe₂), 1.12 (6H, d, ³J = 6.4 Hz, κ²-NCHMe₂), 1.09 (6H, d, ³J = 6.9 Hz, κ¹-NCHMe₂), 0.74 (6H, d, ³J = 6.4 Hz, κ²-NCHMe₂) ppm. ¹³C-{¹H} NMR (CD₂Cl₂, 75.4 MHz, 293 K): 170.0 (MeC(NⁱPr₂)), 168.5 (NC(NⁱPr₂)Ph), 148.7 (br d, ¹J_{CF} = 241.7 Hz, o-C₆F₅), 139.0 (br d, ¹J_{CF} = 245.1 Hz, p-C₆F₅), 137.4 (i-C₆H₅), 136.9 (br d, ¹J_{CF} = 244.4 Hz, m-C₆F₅), 130.4 (C₅Me₃), 130.1 (o-C₆H₅), 129.4 (m-C₆H₅), 127.1 (p-C₆H₅), 51.5 (κ²-NCHMe₂), 49.4 (br, κ¹-NCHMe₂), 25.8 (κ²-NCHMe₂), 24.9 (κ²-NCHMe₂), 22.2 (br, κ¹-NCHMe₂), 20.7 (κ¹-NCHMe₂), 13.9 (MeC(NⁱPr₂)), 13.5 (C₅Me₃) ppm. ¹⁹F NMR (CD₂Cl₂, 282.1 MHz, 293 K): -133.0 (m, o-C₆F₅), -163.8 (m, p-C₆F₅), -167.6 (m, m-C₆F₅) ppm. ¹¹B NMR (CD₂Cl₂, 96.2 MHz, 293 K): -16.5 ppm. IR (NaCl plates, Nujol mull, cm⁻¹): 1643 (m), 1596 (w), 1557 (w), 1540 (m), 1514 (s), 1339 (w), 1311 (w), 1210 (w), 1151 (w), 1085 (s), 1023 (m), 980 (s), 803 (m), 775 (w), 756 (w), 683 (w), 668 (w). Anal. found (calcd. for C₅₅H₅₁BF₂₀N₄Ti): C, 54.51 (57.74); H, 4.13 (4.26); N, 4.78 (4.64)%.

■ ASSOCIATED CONTENT

Supporting Information

The Supporting Information is available free of charge on the ACS Publications website at DOI: 10.1021/acs.organomet.7b00225.

Synthesis details, characterization data, and polymerization results (PDF)

Computed Cartesian coordinates of all molecules reported in this study (XYZ)

Accession Codes

CCDC 1498829–1498843 contain the supplementary crystallographic data for this paper. These data can be obtained free of charge via www.ccdc.cam.ac.uk/data_request/cif, or by emailing data_request@ccdc.cam.ac.uk, or by contacting The Cambridge Crystallographic Data Centre, 12 Union Road, Cambridge CB2 1EZ, UK; fax: +44 1223 336033.

■ AUTHOR INFORMATION

Corresponding Authors

*E-mail: alexandra.berthoud@arlanxeo.com (A.B.).

*E-mail: philip.mountford@chem.ox.ac.uk (P.M.).

ORCID

Philip Mountford: 0000-0001-9869-9902

Notes

The authors declare no competing financial interest.

■ ACKNOWLEDGMENTS

This work was funded by Arlanxeo Netherlands B.V. We thank Drs. M. P. Blake, M. G. Cushion, and A. D. Schwarz for help with some of the crystallography, and we thank the University of Oxford's Advanced Research Computing facility for super-computer access and other resources.

■ REFERENCES

- (a) Resconi, L.; Chadwick, J. C.; Cavallo, L. Olefin polymerizations with Group 4 metal catalysts. In *Comprehensive Organometallic Chemistry III*; Crabtree, R. H., Mingos, D. M., Eds.; Elsevier: Oxford, 2007; Vol. 4. (b) Coates, G. W. *Chem. Rev.* **2000**, *100*, 1223–1252. (c) Ittel, S. D.; Johnson, L. K.; Brookhart, M. *Chem. Rev.* **2000**, *100*, 1169–1203. (d) Baier, M. C.; Zuideveld, M.; Mecking, S. *Angew. Chem., Int. Ed.* **2014**, *53*, 9722–9744. (e) Klosin, J.; Fontaine, P. P.; Figueroa, R. *Acc. Chem. Res.* **2015**, *48*, 2004–2016. (f) Collins, R. A.; Russell, A. F.; Mountford, P. *Appl. Petrochem. Res.* **2015**, *5*, 153–171.
- (a) Brintzinger, H. H.; Fischer, D.; Mülhaupt, R.; Rieger, B.; Waymouth, R. M. *Angew. Chem., Int. Ed. Engl.* **1995**, *34*, 1143–1170. (b) Bochmann, M. J. *Chem. Soc., Dalton Trans.* **1996**, 255–270. (c) Janiak, C. Metallocene catalysts for olefin polymerisation. In

- Metalloenes: Synthesis, Reactivity, Applications*; Togni, A., Halterman, R. L., Eds.; Wiley-VCH: New York, 1998; Vol. 2, p 547–590.
- (d) Kaminsky, W. *J. Chem. Soc., Dalton Trans.* **1998**, 1413–1418.
- (e) Resconi, L.; Cavallo, L.; Fait, A.; Piemontesi, F. *Chem. Rev.* **2000**, *100*, 1253–1346.
- (3) (a) McKnight, A. L.; Waymouth, R. M. *Chem. Rev.* **1998**, *98*, 2587–2598. (b) Braunschweig, H.; Breitling, F. M. *Coord. Chem. Rev.* **2006**, *250*, 2691–2720.
- (4) (a) Nomura, K. *Dalton Trans.* **2009**, 0, 8811–8823. (b) Nomura, K.; Liu, J. *Dalton Trans.* **2011**, 40, 7666–7682.
- (5) (a) Nomura, K.; Naga, N.; Miki, M.; Yanagi, K.; Imai, A. *Organometallics* **1998**, *17*, 2152–2154. (b) Firth, A. V.; Stewart, J. C.; Hoskin, A. J.; Stephan, D. W. *J. Organomet. Chem.* **1999**, *591*, 185–193. (c) Nomura, K.; Tsubota, M.; Fujiki, M. *Macromolecules* **2003**, *36*, 3797–3799. (d) Kim, T.-J.; Kim, S.-K.; Kim, B.-J.; Son, H.-J.; Hahn, J. S.; Cheong, M.; Mitoraj, M.; Srebro, M.; Piękoś, E.; Michalak, A.; Kang, S. O. *Chem. - Eur. J.* **2010**, *16*, 5630–5644.
- (6) (a) Stephan, D. W.; Guérin, F.; Spence, R. E. v. H.; Koch, L.; Gao, X.; Brown, S. J.; Swabey, J. W.; Wang, Q.; Xu, W.; Zoricak, P.; Harrison, D. G. *Organometallics* **1999**, *18*, 2046–2048. (b) Stephan, D. W. *Organometallics* **2005**, *24*, 2548–2560.
- (7) (a) Kretschmer, W. P.; Dijkhuis, C.; Meetsma, A.; Hessen, B.; Teuben, J. H. *Chem. Commun.* **2002**, 608–609. (b) Haas, I.; Hübner, C.; Kretschmer, W. P.; Kempe, R. *Chem. - Eur. J.* **2013**, *19*, 9132–9136. (c) Wu, X.; Tamm, M. *Coord. Chem. Rev.* **2014**, *260*, 116–138. (d) Nomura, K.; Patamma, S.; Matsuda, H.; Katao, S.; Tsutsumi, K.; Fukuda, H. *RSC Adv.* **2015**, *5*, 64503–64513.
- (8) (a) Zhang, S.; Piers, W. E.; Gao, X.; Parvez, M. J. *Am. Chem. Soc.* **2000**, *122*, 5499–5509. (b) Nomura, K.; Fujita, K.; Fujiki, M. *J. Mol. Catal. A: Chem.* **2004**, *220*, 133–144. (c) Ferreira, M. J.; Martins, A. M. *Coord. Chem. Rev.* **2006**, *250*, 118–132.
- (9) (a) Ijpeij, E. G.; Zuideveld, M. A.; Arts, H. J.; Van Doremaele, G. H. J. Zwitterionic amidine polyolefin polymerization catalysts. WO2007059881A1, 2007. (b) Ijpeij, E. G.; Windmuller, P. J. H.; Arts, H. J.; Van der Burgt, F.; Van Doremaele, G. H. J.; Zuideveld, M. A. WO/2005/090418, 2005. (c) Berthoud, A.; Van Doremaele, G. H. J.; Quiroga Norambuena, V.; Scott, R. T. W.; Zuideveld, M. A.; Arts, H. J. EP2816050B2816051, 2013. (d) Ijpeij, E. G.; Coussens, B.; Zuideveld, M. A.; van Doremaele, G. H. J.; Mountford, P.; Lutz, M.; Spek, A. L. *Chem. Commun.* **2010**, 46, 3339–3341.
- (10) (a) Britovsek, G. J. P.; Gibson, V. C.; Wass, D. F. *Angew. Chem., Int. Ed.* **1999**, *38*, 428–447. (b) Kempe, R. *Angew. Chem., Int. Ed.* **2000**, *39*, 468. (c) Gibson, V. C.; Spitzmesser, S. K. *Chem. Rev.* **2003**, *103*, 283–315. (d) Redshaw, C.; Tang, Y. *Chem. Soc. Rev.* **2012**, *41*, 4484–4510.
- (11) (a) Fujita, T.; Makio, H. Polymerization of Alkenes. In *Comprehensive Organometallic Chemistry III*; Mingos, D. M., Crabtree, R. H., Eds.; Elsevier: Oxford, 2007; Vol. 11, pp 691–734. (b) Makio, H.; Terao, H.; Iwashita, A.; Fujita, T. *Chem. Rev.* **2011**, *111*, 2363–2449. (c) Carpentier, J. F.; Kirillov, E.; Sarazin, Y. Metal Phenolates as Polymerization Catalysts. In *PATAI'S Chemistry of Functional Groups*; Zabicky, J., Ed.; John Wiley & Sons, Ltd: 2013.
- (12) (a) Bolton, P. D.; Mountford, P. *Adv. Synth. Catal.* **2005**, *347*, 355–366. (b) Bolton, P. D.; Clot, E.; Cowley, A. R.; Mountford, P. *J. Am. Chem. Soc.* **2006**, *128*, 15005–15018. (c) Bolton, P. D.; Adams, N.; Clot, E.; Cowley, A. R.; Wilson, P. J.; Schroeder, M.; Mountford, P. *Organometallics* **2006**, *25*, 5549–5565. (d) Bigmore, H. R.; Dubberley, S. R.; Kranenburg, M.; Lawrence, S. C.; Sealey, A. J.; Selby, J. D.; Zuideveld, M. A.; Cowley, A. R.; Mountford, P. *Chem. Commun.* **2006**, 436–438.
- (13) Bolton, P. D.; Clot, E.; Adams, N.; Dubberley, S. R.; Cowley, A. R.; Mountford, P. *Organometallics* **2006**, *25*, 2806–2825.
- (14) (a) Delferro, M.; Marks, T. J. *Chem. Rev.* **2011**, *111*, 2450–2485. (b) Stürzel, M.; Mihan, S.; Mühlaupt, R. *Chem. Rev.* **2016**, *116*, 1398–1433. (c) McInnis, J. P.; Delferro, M.; Marks, T. J. *Acc. Chem. Res.* **2014**, *47*, 2545–2557.
- (15) (a) Li, H.; Li, L.; Marks, T. J. *Angew. Chem., Int. Ed.* **2004**, *43*, 4937–4940. (b) Li, H.; Stern, C. L.; Marks, T. J. *Macromolecules* **2005**, *38*, 9015–9027. (c) Noh, S. K.; Kim, S.; Yang, Y.; Lyoo, W. S.; Lee, D.-H. *Eur. Polym. J.* **2004**, *40*, 227–235.
- (16) Li, L.; Metz, M. V.; Li, H.; Chen, M.-C.; Marks, T. J.; Liable-Sands, L.; Rheingold, A. L. *J. Am. Chem. Soc.* **2002**, *124*, 12725–12741.
- (17) (a) Caporaso, L.; Izzo, L.; Sisti, I.; Oliva, L. *Macromolecules* **2002**, *35*, 4866–4870. (b) Salata, M. R.; Marks, T. J. *J. Am. Chem. Soc.* **2008**, *130*, 12–13. (c) Salata, M. R.; Marks, T. J. *Macromolecules* **2009**, *42*, 1920–1933. (d) Li, H.; Li, L.; Schwartz, D. J.; Metz, M. V.; Marks, T. J.; Liable-Sands, L.; Rheingold, A. L. *J. Am. Chem. Soc.* **2005**, *127*, 14756–14768. (e) Li, H.; Li, L.; Marks, T. J.; Liable-Sands, L.; Rheingold, A. L. *J. Am. Chem. Soc.* **2003**, *125*, 10788–10789.
- (18) (a) Guo, N.; Stern, C. L.; Marks, T. J. *J. Am. Chem. Soc.* **2008**, *130*, 2246–2261. (b) Guo, N.; Li, L.; Marks, T. J. *J. Am. Chem. Soc.* **2004**, *126*, 6542–6543. (c) Radlauer, M. R.; Agapie, T. *Organometallics* **2014**, *33*, 3247–3250.
- (19) Motta, A.; Fragalà, I. L.; Marks, T. J. *J. Am. Chem. Soc.* **2009**, *131*, 3974–3984.
- (20) *Arlanxeo Home Page*. <http://www.arlanxeo.com>.
- (21) (a) *Keltan*. <http://www.keltan.com/en/home>. (b) van Doremaele, G. H. J.; van Duin, M.; Valla, M.; Berthoud, A. *J. Polym. Sci. A: Polym. Chem.* **2017**, in press.
- (22) Coe, B. J.; Jones, C. J.; McCleverty, J. A.; Bloor, D.; Cross, G. J. *Organomet. Chem.* **1994**, *464*, 225–232.
- (23) Hansch, C.; Leo, A.; Taft, R. W. *Chem. Rev.* **1991**, *91*, 165–195.
- (24) Fletcher, D. A.; McMeeking, R. F.; Parkin, D. J. *Chem. Inf. Comput. Sci.* **1996**, *36*, 746–759.
- (25) Hagadorn, J. R.; Arnold, J. *Organometallics* **1998**, *17*, 1355–1368.
- (26) (a) Hazari, N.; Mountford, P. *Acc. Chem. Res.* **2005**, *38*, 839–849. (b) Mountford, P. *Chem. Commun.* **1997**, 2127–2134.
- (27) Allen, F. H.; Kennard, O.; Galloy, J. J.; Johnson, O.; Watson, D. G. *Chem. Des. Autom. News* **1993**, 8, 31.
- (28) Dias, A. R.; Duarte, M. T.; Fernandes, A. C.; Fernandes, S.; Marques, M. M.; Martins, A. M.; da Silva, J. F.; Rodrigues, S. S. J. *Organomet. Chem.* **2004**, *689*, 203–213.
- (29) Bader, R. F. W. *Atoms in Molecules: A Quantum Theory*; Oxford University Press: Oxford, 1990.
- (30) (a) Bochmann, M. *Organometallics* **2010**, *29*, 4711–4740. (b) Chen, E. Y.-X.; Marks, T. J. *Chem. Rev.* **2000**, *100*, 1391–1434. (c) Jordan, R. F. *Adv. Organomet. Chem.* **1991**, *32*, 325–387.
- (31) Owen, C. T.; Bolton, P. D.; Cowley, A. R.; Mountford, P. *Organometallics* **2007**, *26*, 83–92.
- (32) Jordan, R. F.; Taylor, D. F.; Baenziger, N. C. *Organometallics* **1990**, *9*, 1546–1557.
- (33) Horton, A. D.; de With, J.; van der Linden, A. J.; van de Weg, H. *Organometallics* **1996**, *15*, 2672–2674.
- (34) (a) Alelyunas, Y. W.; Jordan, R. F.; Echols, S. F.; Borkowsky, S. L.; Bradley, P. K. *Organometallics* **1991**, *10*, 1406–1416. (b) Bochmann, M.; Wilson, L. M.; Hursthouse, M. B.; Motevalli, M. *Organometallics* **1988**, *7*, 1148–1154. (c) Bolton, P. D.; Feliz, M.; Cowley, A. R.; Clot, E.; Mountford, P. *Organometallics* **2008**, *27*, 6096–6110.
- (35) (a) Bochmann, M.; Wilson, L. M. *J. Chem. Soc., Chem. Commun.* **1986**, 1610–1611. (b) Bochmann, M.; Wilson, L. M.; Hursthouse, M. B.; Short, R. L. *Organometallics* **1987**, *6*, 2556–2563.
- (36) (a) Ewart, S. W.; Parent, M. A.; Baird, M. C. *J. Polym. Sci., Part A: Polym. Chem.* **1999**, *37*, 4386–4389. (b) Kissin, Y. V.; Mink, R. I.; Nowlin, T. E.; Brandolini, A. J. *J. Polym. Sci., Part A: Polym. Chem.* **1999**, *37*, 4281–4294. (c) Mori, H.; Endo, M.; Terano, M. *J. Mol. Catal. A: Chem.* **1999**, *145*, 211–220.
- (37) (a) Adams, N.; Arts, H. J.; Bolton, P. D.; Cowell, D.; Dubberley, S. R.; Friederichs, N.; Grant, C. M.; Kranenburg, M.; Sealey, A. J.; Wang, B.; Wilson, P. J.; Zuideveld, M.; Blake, A. J.; Schröder, M.; Mountford, P. *Organometallics* **2006**, *25*, 3888–3903. (b) Busico, V.; Cipullo, R.; Cutillo, F.; Friederichs, N.; Ronca, S.; Wang, B. *J. Am. Chem. Soc.* **2003**, *125*, 12402–12403.
- (38) Yang, X.; Stern, C. L.; Marks, T. J. *J. Am. Chem. Soc.* **1991**, *113*, 3623–3625.
- (39) Chen, E. Y.-X.; Marks, T. J. *Chem. Rev.* **2000**, *100*, 1391–1434.
- (40) Pengborn, A. B.; Giardello, M. A.; Grubbs, R. H.; Rosen, R. K.; Timmers, F. J. *Organometallics* **1996**, *15*, 1518–1520.